RESEARCH ARTICLE

The PRK/Rubisco shunt strongly influences Arabidopsis seed metabolism and oil accumulation, affecting more than carbon recycling

Gabriel Deslandes-Hérold[1,4], Martina Zanella[1,5], Erik Solhaug[1,6], Michaela Fischer-Stettler[1], Mayank Sharma[1], Léo Buergy[1,7], Cornelia Herrfurth[2,3], Maite Colinas[1,8], Ivo Feussner[2,3], Melanie R. Abt[1], Samuel C. Zeeman[1]*

[1] Institute of Molecular Plant Biology, ETH Zurich, CH-8092 Zurich, Switzerland

[2] Department for Plant Biochemistry, Albrecht von Haller Institute for Plant Sciences and Göttingen Center for Molecular Biosciences (GZMB), University of Göttingen, D-37077 Göttingen, Germany

[3] Service Unit for Metabolomics and Lipidomics, Göttingen Center for Molecular Biosciences (GZMB), University of Göttingen, D-37077 Göttingen, Germany

[4] Present address: Institute of Plant Sciences, University of Bern, CH-3013 Bern, Switzerland

[5] Present address: Functional Genomics Center Zurich, ETH Zurich, CH-8057 Zurich, Switzerland

[6] Present address: Institute of Integrative Biology, ETH Zurich, CH-8092 Zurich, Switzerland

[7] Present address: Ecole Polytechnique Fédérale de Lausanne (EPFL), Lausanne, Switzerland

[8] Present address: Department of Natural Product Biosynthesis, Max Planck Institute for Chemical Ecology, Jena, D-07745 Jena, Germany

*Address correspondence to szeeman@ethz.ch

Short title: The PRK/Rubisco shunt in green oilseeds

Abstract
The carbon efficiency of storage lipid biosynthesis from imported sucrose in green Brassicaceae seeds is proposed to be enhanced by the PRK/Rubisco shunt, in which ribulose 1,5-bisphosphate carboxylase/oxygenase (Rubisco) acts outside the context of the Calvin-Benson-Bassham cycle to recycle CO_2 molecules released during fatty acid synthesis. This pathway utilizes metabolites generated by the nonoxidative steps of the pentose phosphate pathway. Photosynthesis provides energy for reactions such as the phosphorylation of ribulose 5-phosphate by phosphoribulokinase (PRK). Here we show that loss of PRK in *Arabidopsis thaliana* (Arabidopsis) blocks photoautotrophic growth and is seedling-lethal. However, seeds containing *prk* embryos develop normally, allowing us to use genetics to assess the importance of the PRK/Rubisco shunt. Compared to nonmutant siblings, *prk* embryos produce one third less lipids—a greater reduction than expected from simply blocking the proposed PRK/Rubisco shunt. However, developing *prk* seeds are also chlorotic and have elevated starch contents compared with their siblings, indicative of secondary effects. Overexpressing PRK did not increase embryo lipid content, but metabolite profiling suggested that Rubisco activity becomes limiting. Overall, our findings show that the

PRK/Rubisco shunt is tightly integrated into the carbon metabolism of green Arabidopsis seeds, and that its manipulation affects seed glycolysis, starch metabolism, and photosynthesis.

IN A NUTSHELL

Background: Light promotes the accumulation of storage lipids during development of oilseeds with green embryos. This has been explained by embryonic photosynthesis generating cofactors that can power an energy-consuming metabolic pathway known as the PRK/Rubisco shunt that is distinct from the Calvin cycle operating in leaves. There is good biochemical evidence for the existence of this pathway in Brassicaceae; however, the extent of its biological significance has not been assessed genetically. Here, we use a refined genetic complementation approach in Arabidopsis to study the role of PRK, specifically in the proposed pathway in its green seeds.

Questions: How can we study the PRK/Rubisco shunt genetically, and what is its quantitative influence on storage oil accumulation in green, developing Arabidopsis seeds?

Findings: As an enzyme integral to the Calvin cycle, the complete loss of PRK is detrimental to plant growth. However, because heterozygous *PRK/prk* plants are phenotypically normal, we used them to establish a plant line generating *prk* embryos in parallel with complemented siblings, which can be differentiated using a fluorescent marker. The absence of PRK throughout embryogenesis reduced the oil content in the embryo by one third; more than expected from theoretical calculations of the contribution of the PRK/Rubisco shunt. Several lines of evidence further indicate tight metabolic integration of the shunt into green embryo photosynthesis and metabolism.

Next steps: Our observations provide insight into the integration of the PRK/Rubisco shunt into Arabidopsis embryo metabolism. We would like to understand better how it is coordinated with pathways leading to other storage compounds, how it is regulated genetically and biochemically, and how this knowledge can help oil crop improvement.

Introduction

Developing plant seeds rely on maternally derived substrates to sustain their metabolism and synthesize the storage compounds that fuel germination and seedling establishment. The cleavage of sucrose obtained from the mother plant yields hexose phosphates that supply metabolic processes such as starch biosynthesis and the respiratory pathways, i.e. glycolysis, the tricarboxylic acid (TCA) cycle, and the oxidative pentose phosphate pathway (OPPP), pathways that generate precursors for amino acid and lipid biosynthesis (Baud et al., 2008). Partitioning among these different pathways during seed development is dynamic and species dependent, resulting in some seeds accumulating starch as the predominant final storage compound (as in many grasses) and others accumulating lipids (as in many Brassicaceae).

The Brassicaceae include many commercially important oilseed species (e.g. *Brassica napus, Brassica rapa*, and *Brassica juncea*) and the widely studied model species *Arabidopsis thaliana* (Arabidopsis). Although the seeds of such species are oil-rich at maturity, they also transiently accumulate starch during development, prior to lipid accumulation (da Silva et al., 1997; Focks and Benning, 1998; Baud et al., 2002). The shift in the utilization of carbon resources during seed filling has been proposed to be the result of several developmental regulators, notably the transcription factor WRINKLED1 (WRI1) (Focks and Benning, 1998; Cernac and Benning, 2004).

Both starch and lipid biosynthesis draw on the hexose phosphate pool in the seed, but they differ significantly with regard to complexity, energy demand, carbon efficiency, as well as the final energy density attained. Starch biosynthesis happens exclusively inside plastids and utilizes ADP-Glucose (ADPGlc), a nucleotide-activated sugar derived directly from the interconversion of hexose phosphates, as substrate (see Pfister and Zeeman, 2016, for a comprehensive review). The numerous steps required for storage lipid biosynthesis are distributed among several cellular locations. Broadly speaking, storage lipid biosynthesis can be divided into three sequential parts: synthesis of the substrate pyruvate by glycolysis, fatty acid (FA) biosynthesis, and triacylglycerol (TAG) assembly.

Both the cytosol and the plastids contain the enzymes to perform glycolysis (Kang and Rawsthorne, 1994). Current evidence from *B. napus* and Arabidopsis suggests that, during seed filling, both the cytosol and plastids may be involved. Cytosolic glycolysis produces phosphoenolpyruvate (PEP) and, to some extent, pyruvate (Pyr), both of which can be imported

1   to fuel the plastidial biogenesis of acetyl-CoA (Eastmond and Rawsthorne, 2000; White et al.,

2   2000; Ruuska et al., 2002; Schwender et al., 2015). Acetyl-CoA is subsequently used by the

3   plastidial acetyl-CoA carboxylase (ACCase), a multisubunit enzyme, to generate malonyl-CoA

4   in a first committed step toward FA biosynthesis (Konishi et al., 1996; Thelen and Ohlrogge,

5   2002). Several sequential enzymatic activities then generate FAs, the majority of which are

6   exported from the plastid. In the endoplasmic reticulum (ER), these exported FAs are transferred

7   onto glycerol-3-phosphate (Gly-3P) to form TAGs, the final lipid storage form (see Baud et al.,

8   2008, and references therein).

9   Lipid biosynthesis requires large amounts of energy (as ATP) and reducing power (as

10   NADH, NADPH), and also releases one molecule of CO_2 at the oxidative decarboxylation of Pyr

11   to acetyl-CoA, catalyzed by pyruvate dehydrogenase (PDH). This reduces the carbon conversion

12   efficiency by one third with respect to starch biosynthesis (Baud and Lepiniec, 2010). Through

13   elegant labelling experiments, Schwender and colleagues demonstrated that in developing

14   Brassicaceae seeds, the Calvin-Benson-Bassham cycle (CBBC) enzymes phosphoribulokinase

15   (PRK) and Rubisco act in a noncanonical metabolic context to recycle the CO_2 released by PDH

16   (Schwender et al., 2004). This PRK/Rubisco shunt utilizes substrates generated by the

17   nonoxidative steps of the PPP, and the carboxylation action of Rubisco generates additional 3-

18   phosphoglycerate (3PGA) while bypassing parts of glycolysis. The increased costs of this

19   pathway, in terms of energy and reductant, are met by photosynthesis in the developing green

20   seeds using the residual light transmitted through the surrounding seed coat and pod wall.

21   This proposed pathway is consistent with earlier findings showing that the photosynthetic

22   electron transport chain is functional in isolated *B. napus* embryos (Asokanthan et al., 1997) and

23   that seed lipid content is positively influenced by light in both *B. napus* and Arabidopsis (Ruuska

24   et al., 2004; Li et al., 2006). Schwender et al. calculated that, in *B. napus*, Rubisco is responsible

25   for up to half of the 3PGA molecules subsequently used for FA biosynthesis. This corresponds to

26   an increased carbon efficiency of 10% compared to using glycolysis as the only source of 3PGA.

27   This value is consistent with the increased carbon conversion efficiency of green *B. napus* seeds

28   compared to nongreen sunflower seeds (Schwender et al., 2004). Interestingly, in later studies,

29   the contribution of Rubisco in the context of developing, green seeds was shown to vary

30   significantly not only between species (25% and 90% of total plastidic 3PGA produced by

31   Rubisco in pennycress and Arabidopsis, respectively (Lonien and Schwender, 2009; Tsogtbaatar

4

1 et al., 2020)) but also between different genotypes of the same species (*B. napus:* between 42-

2 68% of 3PGA molecules originating from Rubisco activity in different entries; Schwender et al.,

3 2015).

4   The above-mentioned discoveries have provided initial insight into the relevance of

5 Rubisco-mediated carbon fixation in the context of green-seed metabolism. Here, we provide

6 genetic evidence for the role of this pathway in Arabidopsis, a close relative of *B. napus*. Using

7 an integrated molecular genetic approach, we modulate the availability of the Rubisco substrate

8 ribulose-1,5-bisphosphate (RuBP) via either elimination or overexpression of PRK. We

9 demonstrate the importance of the PRK/Rubisco shunt on seed oil accumulation and we show

10 that Rubisco-mediated CO_2 recycling is tightly integrated with carbon and energy metabolism in

11 the embryos of green oilseeds.

12

13 **Results**

14 *Mutations in PRK are seedling lethal*

15 We sought to study the influence of the PRK/Rubisco shunt on Arabidopsis seed lipid

16 metabolism using a genetic approach. Rubisco is a multisubunit enzyme consisting of eight

17 catalytic large subunits and eight small subunits. The large subunit is encoded by the plastid

18 genome, and multiple nuclear genes encode the small subunits (Andersson and Backlund, 2008).

19 Given this complexity, direct genetic manipulation of Rubisco is not straightforward. In contrast,

20 PRK, the enzyme that phosphorylates ribulose-5-phosphate (Ru5P) to generate the Rubisco

21 substrate RuBP, is encoded by a single nuclear gene (locus AT1G32060) and thus is much more

22 easily amenable to genetic manipulation. We therefore used *prk* mutants to study the

23 involvement of the PRK/Rubisco shunt in green Arabidopsis seeds.

24   Previously, PRK was repressed in tobacco (*Nicotiana tabacum* L.) to very low levels,

25 resulting in reductions in CO_2 assimilation rates, in chlorophyll content, and in relative growth

26 rate (Paul et al., 1995; Banks et al., 1999). These studies suggested that a relatively small fraction

27 of the endogenous PRK is necessary to sustain metabolism under ambient conditions. However,

28 being a core enzyme of the CBBC, the complete loss of PRK should severely compromise plant

29 viability. We obtained two heterozygous Arabidopsis mutant lines, *prk-1* (GK-117E07; a T-DNA

30 insertion line, hereafter referred to as *prk*) and *prk-2* (RIKEN-pst19435; a transposon tagged

31 line). Using PCR-based genotyping and DNA sequencing, we pinpointed their insertions to the

1 fourth (*prk-1*) and second (*prk-2*) exon of *PRK*, respectively (Figure 1A). These heterozygous

2 plants were morphologically indistinguishable from their respective wild types. Both lines

3 produced seeds that were uniform in appearance and germination. However, while three quarters

4 of the seedlings developed in a wild-type-like fashion, one quarter of them became pale

5 immediately after germination and arrested growth at the cotyledon stage of vegetative growth

6 (Figure 1B; Table 1). Using PCR-based genotyping, we confirmed that, as expected, these pale

7 seedlings were homozygous for the T-DNA insertion in the *PRK* locus.

8

9 *Generation of lines with visually assessable PRK segregation*

10 Although the striking growth phenotype of the homozygous *prk* offspring became readily

11 apparent after germination, there was no obvious visible effect on the developing seeds of the

12 heterozygous mother plants. In order to study the specific metabolic effects of a loss of PRK, we

13 designed a genetic complementation strategy to be able to identify homozygous *prk* seeds *in situ*

14 and compare them to their complemented siblings. Therefore, we transformed heterozygous *prk*

15 plants with a construct encoding PRK with a C-terminal YFP tag under the control of the

16 endogenous *PRK* promoter, hereafter referred to as PRK_{pro}:*PRK-YFP*. This construct was able to

17 complement the *prk* phenotype: several transgenic lines with a confirmed homozygous *prk*

18 background, but a normal growth phenotype and morphology, could be isolated either directly

19 from the T_1 or from the T_2 generation. We applied very stringent selection criteria (see Materials

20 and Methods for details) to identify the line best suited for further detailed analysis.

21 In brief, for each independent transformant line, we screened seedlings on selective

22 media, looking for a segregation ratio of 3:1 (resistant:sensitive), which is indicative of a single-

23 locus insertion of the PRK_{pro}:*PRK-YFP* rescue construct. We then used Illumina whole-genome

24 sequencing to simultaneously rule out those with multiple insertions and determine each

25 integration site. Primers specific to these genomic sites and the transgene borders were designed,

26 and the remaining transformants were genotyped to exclude those with tandem inverted

27 insertions. We chose a line with a single-locus transgene insertion in an intergenic region on

28 chromosome 3 (unlinked to the endogenous *PRK* gene). Finally, we raised antibodies against the

29 recombinant PRK protein and confirmed by immunoblotting that the selected line expressed

30 PRK-YFP to levels similar to the endogenous PRK in the wild type (Supplemental Figure 1A).

6

1 Notably, this line, which we refer to as prkCOMP hereafter, has a wild type-like overall

2 phenotypic appearance (Supplemental Figure 1B).

3 We maintained prkCOMP in a hemizygous state for the introduced *PRK_{pro}:PRK-YFP*

4 transgene, but homozygous for the *prk* background. Consequently, this line gives rise to seed

5 populations segregating for the complementation construct. We observed that one quarter of the

6 germinated seeds developed into pale, growth-arrested seedlings, as was already observed for the

7 heterozygous *prk* mutant. We confirmed the absence of the endogenous PRK protein and the

8 segregation of the PRK-YFP fusion protein by immunoblotting with antibodies recognizing PRK

9 and the YFP tag (Figure 2A). For this, total protein extracts from both normal green seedlings

10 and pale seedlings derived from prkCOMP were used. The band corresponding to endogenous

11 PRK, visible in the wild-type control, was absent in all prkCOMP-derived seedlings. Both

12 antibodies detected a band at the size expected for the mature PRK-YFP fusion protein in the

13 green prkCOMP-derived seedlings (68 kDa after cleavage of the transit peptide), but not in the

14 pale ones. These results confirmed both the presence of the *prk* mutant background and the

15 successful complementation strategy. Further, the blot using anti-PRK antibodies confirmed

16 again that PRK-YFP was present at comparable levels to the endogenous PRK present in the

17 wild-type seedlings.

18 We next tested whether we could distinguish between the segregating genotypes at the

19 seed stage based on the fluorescence of the PRK-YFP protein. Indeed, using a simple

20 fluorescence microscope, YFP-fluorescent and non-YFP-fluorescent seeds could readily be

21 distinguished within each silique (Figure 2B). Seeds were sorted into three populations: 23.6%

22 (median ratio of seeds per silique) fluoresced red (R) due to chlorophyll autofluorescence, 56.4%

23 fluoresced yellow (Y) and 20.0% showed high yellow fluorescence (YY). Seeds classified as R

24 presumably represent the noncomplemented *prk* population, while those classified as Y and YY

25 likely correspond to those hemi- or homozygous for *PRK_{pro}:PRK-YFP*, respectively. However,

26 the latter sub-classification was more difficult to assign, possibly explaining the slight deviation

27 from the expected number of Y and YY seeds. Nevertheless, immunoblot analyses that showed

28 high and intermediate levels of PRK-YFP protein in extracts prepared from YY and Y seeds,

29 respectively (and none in R seeds), support this assumption (Figure 2C).

30

7

Loss of PRK in developing green seeds depletes Rubisco substrates, leads to reduced lipid accumulation, and affects chlorophyll content

We used the segregating offspring from prkCOMP to determine the effects of the absence of PRK on seed metabolites and lipid content. Green developing seeds (10 d after flowering; DAF) were sorted according to their fluorescence as described above. R, Y and YY seeds from single siliques were separately flash-frozen in liquid N_2. Samples were extracted and the levels of primary metabolites measured using LC-MS. Clustering of the resulting data via principal component analysis (PCA) revealed that each seed class had a distinct metabolite profile (Figure 3, Supplemental Data Set 1). The R samples clustered apart from the Y and YY samples, which also separate from each other, indicating that the copy number of the *PRK$_{pro}$:PRK-YFP* rescue construct (presumably reflecting the level of PRK activity) influenced the metabolome of the seeds.

We compared the metabolite levels in the R (corresponding to *prk*) and YY (corresponding to fully complemented) seeds. Consistent with a block at the PRK step, the content of several pentose phosphate pathway metabolites upstream of the PRK/Rubisco shunt, notably sedoheptulose-7P (Sed7P), ribose-5P (Rib5P), and xylulose-5P (Xyl5P), were significantly increased in R compared to YY seeds, although surprisingly, the PRK substrate Ru5P was not (Figure 4, Supplemental Data Set 1). Conversely, the PRK product RuBP was barely measurable (below the dynamic range of the calibration curve for all R samples; see Materials and Methods section for details), and metabolites of the glycolytic sequence including the Rubisco product 3PGA, PEP, and Pyr, were strongly decreased in R seeds. These data provide direct evidence that PRK and Rubisco are operating in green, developing Arabidopsis seeds.

Because Pyr is converted to the FA precursor acetyl-CoA, we next measured if R seeds had reduced levels of FAs in mature embryos. While it was possible to sort seeds according to their fluorescence when they were green, with a translucent seed coat, it was more difficult when the seeds were mature. Here, direct visual phenotyping was prevented by the darkened, pigmented seed coat. Therefore, after a brief (2-4 h at 4°C) period of imbibition, the seed coat was removed prior to fluorescence screening. TAG contents have previously been observed to remain stable for 16 h of imbibition at 4°C (Li et al., 2006). We sorted the embryos according to their fluorescence, which could easily be designated YFP-fluorescent or non-YFP-fluorescent.

8

1   However, as it was more difficult to distinguish between Y and YY classes, all YFP-fluorescent

2   embryos were pooled (referred to as Y/YY hereafter). Lipids were quantified as fatty acid methyl

3   esters (FAMEs) (Lang et al., 2011) upon methanolysis and were detected using gas

4   chromatography coupled to a flame ionization detector (GC-FID) (Miquel and Browse, 1992).

5   Remarkably, R embryos had a highly reproducible ~34% reduction of total lipid content

6   compared to Y/YY embryos (Figure 5A). We also analysed excised embryos from Col-0 wild-

7   type plants, whose lipid content was in a similar range as that of complemented PRK-YFP

8   embryos, suggesting that our complementation strategy adequately restores a wild-type-like

9   status.

10   The overall FA profiles were similar to those found in previous reports (Lemieux et al.,

11   1990). However, the absence of PRK disproportionally affected specific FA species.

12   Interestingly, the proportions of 18:1 and 18:2 FAs were significantly reduced in R compared to

13   Y/YY embryos, whereas 18:3 was increased (Supplemental Data Set 2, Supplemental Table 1).

14   The proportions of very long-chain FAs 20:2, 20:3 and 22:1 were increased, although these are

15   minor. In contrast, the proportion of the major FA species 20:1, representing a marker FA of

16   TAG in Arabidopsis (Lemieux et al., 1990), was normal, suggesting that oil storage was not

17   specifically affected.

18   The proposed contribution of PRK/Rubisco to FA biosynthesis in green seeds is

19   dependent on ATP and reducing equivalents derived from the photosynthetic electron transport

20   chain. Thus, we next tested both whether the intensity of light that siliques were exposed to

21   during seed development influenced the accumulation of lipids, and whether this influence was

22   conditional on the presence of PRK. For this, prkCOMP plants were grown in high light (300

23    $\mu mol \ m^{-2} \ s^{-1}$; twice the normal the light intensity) and subsequently subjected to three different

24   treatments during seed development: 1. a reduction to normal light (NL: entire plant shielded

25   with a grey filter that reduced light intensity by 50%); 2. normal light for maternal source tissues,

26   high light for siliques (NLr: rosette shielded with a grey filter that reduced light intensity by

27   50%); and 3., high-light (HL: no filter applied). Seeds were harvested, sorted, and total FA

28   contents measured as described above. As expected for a light-supported process, FA

29   accumulation in Y/YY and control Col-0 wild-type embryos positively correlated with the light

30   intensity experienced during seed maturation. Reducing the illumination of the rosette did not

31   influence lipid accumulation in Y/YY, but interestingly, a small reduction was observed for

9

wild-type embryos. This may reflect an influence of maternal *PRK* copy number (two in the wild type versus the one in prkCOMP) on accumulation of seed storage compounds under higher light. In contrast, the FA content of dissected R embryos did not differ significantly between any of the treatments (Figure 5B, Supplemental Data Set 3). Together, these measurements confirm that the process of lipid biosynthesis in Arabidopsis embryos is supported by light, and that this support is dependent on PRK.

Intriguingly, whenever sorting developing green prkCOMP seeds, we noticed that R seeds, in addition to being devoid of yellow fluorescence, appeared slightly paler than Y or YY seeds under brightfield microscopy conditions (Figure 2B). We therefore measured chlorophyll levels and indeed found that R seeds had a reduced total chlorophyll content compared to their YY siblings (Figure 6, Supplemental Data Set 4). This suggests that the loss of PRK has secondary effects on the photosynthetic capacity.

Eliminating the flux through PRK/Rubisco perturbs the starch/lipid balance in prk *embryos*

When analysing our LC/MS measurements on sorted developing prkCOMP seeds, we noticed that the total pool of interconvertible hexose phosphates (Glc6P, Glc1P, and Fru6P) was significantly increased in R seeds relative to YY seeds (See Supplemental Data Set 1). Hexose phosphates not only feed into glycolysis and the PRK/Rubisco shunt, but also supply plastidial starch biosynthesis via the generation of ADPGlc, whose level was also increased (Figure 4). Arabidopsis embryos are known to transiently store starch around 3-14 DAF (Baud et al., 2002), but this starch is almost completely degraded again and replaced by lipids once seeds reach a mature stage (approximately 20 DAF). To assess whether this metabolic branch was affected by the loss of the PRK/Rubisco shunt, we harvested and sorted green prkCOMP seeds at different stages of development, removed their seed coats to facilitate chemical fixation, and embedded them in plastic resin. We then investigated the cellular contents of R and YY embryos using transmission electron microscopy (TEM). As expected from our earlier findings, R embryos had fewer and smaller lipid bodies than did their complemented siblings (Figure 7A and B). The plastids of both types of embryos still contained starch granules at 13 DAF, but while most of this starch had disappeared in YY embryos at 16 DAF, granules were still present in R embryos, suggesting that the turnover of starch was delayed.

We quantitated the starch content in sorted green prkCOMP seeds in order to substantiate our TEM observations. Starch in the seeds was solubilized, enzymatically digested, and the resulting free glucose was quantified as described previously (Solhaug et al., 2019). Surprisingly, there was appreciable variation in seed starch content, from 3 to 53 (R) and 1 to 50 nmol (YY) glucose equivalents seed^{-1} in the samples, depending on the silique from which they were taken (Supplemental Data Set 5). We assume this was due to slight differences in the developmental stages of the siliques at the time of harvest. To correct for this, we normalized the starch content of each R sample to the value of the respective YY sample from the same silique. The resulting fold changes indicated a significantly increased seed starch content for R seeds (Figure 7C). Together with the increased hexose phosphate and ADPGlc content and the retention of starch granules in TEM observations, this suggests that the biosynthesis of seed starch is upregulated in the absence of PRK. However, it is also possible that starch is not properly mobilized during later development.

Increased flux through PRK/Rubisco does not translate into increased lipid content

Considering that the absence of PRK resulted in a decreased glycolytic intermediate content, reduced lipid content, and the loss of light-responsive lipid accumulation, we tested whether an increase in PRK abundance would have the opposite effect. We isolated a line carrying the same *PRK$_{pro}$:PRK-YFP* transgene insert as prkCOMP in a hemizygous state in the wild-type genetic background (Supplemental Figure 1B). This line also produces seed populations with observable PRK-YFP segregation, which in this case allowed us to compare metabolite contents of seeds with enhanced PRK expression (because *PRK$_{pro}$:PRK-YFP* is expressed in addition to endogenous PRK) compared to wild-type seeds in the same silique. We refer to this line as PRKOX.

We first assessed metabolite levels in sorted, green PRKOX seeds using LC-MS. Compared to their wild-type siblings, YY PRKOX seeds had highly elevated levels of the PRK reaction product RuBP, suggesting that PRK activity was indeed increased (Supplemental Figure 2, Supplemental Data Set 6). Unexpectedly, the level of the PRK substrate Ru5P was also elevated in the YY seeds. The reason for this is unclear, but some hydrolysis of RuBP to Ru5P may have occurred during extraction and caused this. The accumulation of RuBP to high levels suggests that Rubisco activity may limit the new flux regime. Nevertheless, levels of

downstream glycolytic metabolites up to Pyr were increased, suggesting that the flux through the PRK/Rubisco shunt was higher in PRKOX YY seeds than in their wild-type siblings. Interestingly, the level of the starch substrate ADPGlc was again strongly increased. This may be the result of high 3PGA levels stimulating AGPase activity (Iglesias et al., 1993). Interestingly, the increases in ADPGlc, 3PGA, PEP, and Pyr in YY PRKOX seeds was contrasted by decreases in FruBP and Gly-3P (not shown in Supplemental Figure 2; see Supplemental Data Set 6A-C), suggesting that the substrates of glycolysis may have been depleted by drawing metabolites through the nonoxidative pentose phosphate pathway for the PRK/Rubisco shunt, and their redirection to ADPGlc through AGPase.

We also tested whether the increased flux through the PRK/Rubisco shunt influenced embryo lipid accumulation. Despite the increased abundance of FA precursors in YY PRKOX seeds, the FA content itself was not measurably increased compared to the FA content in their wild-type siblings (Figure 5A), suggesting the presence of additional metabolic bottlenecks downstream in lipid biosynthesis.

Discussion

Elimination of PRK causes a seedling-lethal phenotype

PRK has been previously targeted by antisense expression in tobacco and the resulting effects were studied mostly with a focus on overall plant growth and photosynthesis (Paul et al., 1995; Banks et al., 1999). These important studies predate the discovery of the PRK/Rubisco shunt. Also, to our knowledge, the specific effects of PRK deficiency on lipid metabolism in the seeds of these lines has not been assessed. Furthermore, we are not aware of any previous investigations into the phenotype of complete loss-of-function mutants of PRK in vascular plants. Not surprisingly, we found that such mutants fail to complete the transition from heterotrophic to photoautotrophic growth and that their development is thus arrested at the cotyledon stage (Figure 1B), as previously seen for other mutants with an impaired CBBC (Carrera et al., 2021).

To study the specific effects of blocking the PRK/Rubisco shunt on seed lipid biosynthesis, we needed to establish an effective and refined genetic complementation strategy. Our prkCOMP line features several characteristics rendering it a suitable tool for detailed genetic analyses. First, each individual hemizygous prkCOMP mother plant produces both offspring that

1 entirely lack PRK and offspring that express PRK to wild-type like levels in all of its siliques.

2 This enables the importance of the PRK/Rubisco shunt to be studied independently of maternal-

3 and/or silique-specific effects. This is crucial, because although green seeds are supplied with

4 resources from the mother plant, they utilize external light to support endogenous processes.

5 Thus, their metabolism is intrinsically responsive to both maternal and environmental influences.

6 Indeed, genetic and environmental factors affecting the metabolic status of the mother plant can

7 strongly influence seed storage compound accumulation (Periappuram et al., 2000; Li et al.,

8 2006; Andriotis et al., 2010; Andriotis et al., 2012). Second, the genotypes of individual

9 offspring developing in prkCOMP siliques can be identified using the YFP tag that is fused to

10 PRK. This allowed us to screen for homozygous rescued seeds and thus minimize differences

11 due to variable PRK expression. Third, similar to the heterozygous *prk* mutants, the prkCOMP

12 line had a growth phenotype similar to wild type plants, despite carrying only a single allele of

13 the rescue construct (Supplemental Figure 1B). It is unlikely that, under normal growth

14 conditions, photosynthesis is limited by a reduced PRK level resulting from a single gene copy,

15 since early experiments on spinach chloroplasts estimated that PRK reached only a small fraction

16 of its maximal activity under physiological conditions (Gardemann et al., 1983). Later, using

17 antisense tobacco lines, measurable reductions in photosynthesis were detected only when PRK

18 was repressed to very low levels, and decreased enzyme abundance correlated with a

19 compensatory increase in its activation state (Paul et al., 1995; Banks et al., 1999). Thus, we can

20 largely exclude the possibility that the prkCOMP line is impaired in providing substrates to its

21 seeds under normal growth conditions, though it remains possible that there is a small effect

22 when grown in high light.

23

24 *The reduction in lipid content in prk embryos exceeds that predicted by the PRK/RUBISCO shunt*

25 Despite the severe effect on seedling growth, the loss of PRK did not visibly affect either seed

26 development or final seed size (Figure 2B). Nevertheless, its loss essentially eliminated the

27 Rubisco substrate RuBP (Figure 4) and blocked the proposed glycolytic bypass acting during

28 lipid synthesis in green seeds. As expected, we observed accumulation of the upstream pentose

29 phosphate pathway metabolites, and downstream FA precursors were depleted. Furthermore,

30 there was a marked decrease in lipid content in mature embryos (Figures 4 and 5). On one hand,

31 this confirms that PRK and Rubisco add to the efficiency of storage lipid metabolism in green

13

1 Arabidopsis seeds. On the other hand, the extent to which this occurs was surprising: Mature *prk*
2 embryos contained 34% less total FA than their PRK-expressing siblings. Interestingly, this is
3 roughly two times higher than earlier estimates of the contribution of the PRK/Rubisco shunt in
4 Arabidopsis (Lonien and Schwender, 2009), and still 1.7 times the maximum that the shunt could
5 theoretically provide, assuming that all imported carbon directed into acetyl-CoA would flow
6 through Rubisco. Because oil represents a major component of mature Arabidopsis seeds (36%
7 by weight; Li et al., 2006), we would expect the observed reduction in FA content to translate
8 into a decreased overall embryo weight, and that the magnitude of decrease would depend on
9 whether any of the carbon originally destined for FA biosynthesis had been redirected into other
10 compounds. However, we did not assess total mature embryo biomass in our experiments,
11 because the prkCOMP seeds can only be sorted at this stage after removal of the seed coat,
12 necessitating seed imbibition.

13 Our data provide further insight that allows us to propose explanations for this
14 unexpectedly strong effect. The activity of the PRK/Rubisco shunt depends on a functional
15 photosynthetic transport chain, and thus the availability of light. Indeed, lipid accumulation in
16 green Brassicaceae seeds has been previously linked to the intensity of illumination experienced
17 by the seed during development (Ruuska et al., 2004). Our experiments applying different
18 intensities of light to maturing Arabidopsis seeds confirm this dependence and show that it is lost
19 in the absence of PRK (Figure 5B). Although the PRK/Rubisco shunt uses only a fraction of the
20 energy needed to operate the CBBC, it is still likely to be a major sink for the products of the
21 photosynthetic electron transport chain in green seeds, together with downstream steps in FA
22 biosynthesis. The loss of PRK could therefore result in an excess of energy and reductant
23 generated by the photosynthetic light reactions; no ATP would be needed for the PRK step, and
24 the depletion of precursors would reduce the rate of FA and thus the rate of lipid biosynthesis.
25 Consequently, excessive reduction of the photosynthetic electron transport chain may occur, with
26 enhanced generation of reactive oxygen species (ROS) and resultant photo-oxidative damage and
27 bleaching (Niyogi, 1999). This is clearly evident in the cotyledons of germinated *prk* seedlings as
28 a result of their inability to run the CBBC. It may also occur in developing *prk* seeds—those
29 originating from our prkCOMP line appeared paler and had less chlorophyll compared to their
30 complemented siblings (Figure 2B; Figure 6). If *prk* seeds indeed suffer from an imbalance

14

between photosynthetic light harvesting and utilisation of this energy, there may be further unanticipated pleiotropic effects contributing to the reduced accumulation of storage compounds.

Our metabolite measurements do not provide sufficient information to assess metabolic fluxes. Nevertheless, the unchanged levels of glycolytic substrates between complemented and non-complemented *prk* seeds (Figure 4) allow us to speculate that one or more of the early steps of glycolysis may have insufficient capacity to channel all carbohydrates obtained from the mother plant to FA biosynthesis. Furthermore, one could imagine that curbing the activity of glycolysis was a necessary evolutionary step to facilitate the alternative flux through the pentose phosphate pathway and PRK/Rubisco shunt, given that the two pathways draw from the same pool of resources. The fact that we also detected an increase in the total pool of hexose phosphates in *prk* seeds supports the idea that maternally derived carbohydrates are not efficiently used. This side effect could further explain our observation that green *prk* seeds have elevated ADPGlc, and at least transiently produce/retain higher levels of starch compared with their PRK-containing siblings; Transiently elevated starch levels were observed in green seeds of the Arabidopsis *wri1* mutant, which feature increased soluble sugar contents alongside much reduced FA biosynthesis (Focks and Benning, 1998).

Consistently, a recent study of *in-vitro* cultured *B. napus* embryos demonstrated the existence of a trade-off between the partitioning of carbon into starch vs. lipids (Schwender et al., 2015). Thus, the blockage in the PRK/Rubisco shunt, together with the increased pool of hexose phosphates, could redirect resources into starch production, further helping to explain the large decrease in partitioning to lipid biosynthesis. However, since starch is synthesized and then degraded within a relatively short time frame during embryo development (Baud et al., 2002), further time-course measurements are needed to provide quantitative information about the changes in carbon allocation to the lipid and starch pools in *prk* seeds, and to understand how this translates into the final starch and lipid composition in the mature seed.

We also cannot exclude the possibility of an active CBBC cycle operating to some extent in developing Arabidopsis embryos. Evidence of CBBC activity in isolated *B. napus* embryos was observed under in vitro conditions at a light intensity of 150 µmol m^{-2} s^{-1} (Goffman et al., 2005). Although this is the same light intensity that we used for our experiments, we would expect the silique wall and seed coat to significantly reduce the light reaching the embryos—only 20-30% of the light is transmitted in the case of *B. napus* (Eastmond et al., 1996; King et al.,

1   1998). It is presently unclear whether these intensities would be sufficient to sustain CBBC

2   activity in vivo. However, any CBBC activity would be abolished in *prk* embryos in addition to

3   the PRK/Rubisco shunt, and this could help explain the higher-than-expected influence on seed

4   oil accumulation.

5   Finally, it is also worth noting that seed production is energetically costly to the mother

6   plant, and its limited resources are divided among the whole population of developing seeds. We

7   cannot exclude the possibility that lower utilization of imported carbohydrate in green *prk* seeds

8   negatively affects resource import (e.g. if sucrose accumulates and inhibits further uptake).

9   Indeed, significantly reduced sucrose uptake has been observed for Arabidopsis *wri1* mutant

10 embryos cultivated in vitro (Lonien and Schwender, 2009). If so, the maternal allocation to seeds

11 of different genotypes may vary, with resources diverted to those seeds capable of utilizing the

12 substrates more efficiently, i.e. those with a stronger sink strength. Such a scenario may combine

13 two effects: first, reduced lipid accumulation in *prk* seeds; and second, increased lipid

14 accumulation in complemented siblings. Such a shift in resource allocation, though likely to be

15 small, may contribute to the larger-than-expected difference in oil content measured between *prk*

16 and wild-type-like embryos.

17

18 *Enhancing the flux through PRK is insufficient to increase lipid accumulation*

19 As a complement to prkCOMP, the PRKOX line allowed us to assess the effects of increased

20 PRK activity in the developing seed. The accumulation of RuBP in YY seeds of this line

21 suggests that Rubisco activity could not keep up with the increased PRK activity and may

22 represent one of the next limiting factors in the pathway. This is somewhat surprising, because

23 transcriptome data from developing Arabidopsis seeds indicated that expression of both PRK and

24 Rubisco are induced at the same time as are many enzymes involved in FA biosynthesis (Ruuska

25 et al., 2002). Furthermore, Rubisco was not only abundant but also highly carbamylated (and

26 thus active) in developing *B. napus* embryos, presumably due to the prevailing high

27 concentration of CO_2 (Ruuska et al., 2004; Hajduch et al., 2006). However, it is still possible that

28 the increase in PRK activity in our PRKOX line is eventually saturating for Rubisco; indeed, we

29 did observe some increases in 3PGA, PEP, and Pyr levels (Supplemental Figure 2), indicating

30 that the PRK/Rubisco shunt may have been more active. The fact that this did not translate to a

31 measurable increase in lipid content may indicate that other steps, possibly located in the

16

downstream FA biosynthesis or subsequent TAG assembly pathways, also limit lipid accumulation (Bates et al., 2013).

Much evidence points towards lipid accumulation being a complex and regulated metabolic process that is reliant on a multitude of enzymatic and environmental factors. Several approaches individually targeting suspected rate-limiting steps of FA biosynthesis had only modest effects, no effects, or even a negative impact on seed oil accumulation in *B. napus* (Verwoert et al., 1995; Roesler et al., 1997; Dehesh et al., 2001). Although in a recent study, seed oil content was significantly increased by overexpression of pea (*Pisum sativum*) α-carboxyltransferase, a subunit of ACCase, in Arabidopsis and camelina (*Camelina sativa*) (Wang et al., 2022), top-down metabolic control analysis suggested that not only plastidial FA biosynthesis, but also the ER-located Kennedy pathway exert control over lipid biosynthesis in oil palm (*Elaeis guineensis* Jacq.) and olive (*Olea europaea* L.) (Ramli et al., 2002). Indeed, overexpression of an Arabidopsis Gly-3P acyltransferase (GPAT9), a yeast (*Saccharomyces cerevisiae*) *lyso*-phosphatidic acid acyltransferase (LPAT), and diacylglycerol acyltransferase (DGAT), catalysing the first, second, and final steps of TAG formation in the ER, respectively, increased seed oil content in *B. napus* and Arabidopsis (Zou et al., 1997; Jako et al., 2001; Taylor et al., 2002; Singer et al., 2016). Increasing the levels of Gly-3P (which forms the backbone of TAGs) by overexpression of a yeast Gly-3P dehydrogenase was also reported to increase oil content (Vigeolas et al., 2007). This is interesting, as we observed that Gly-3P levels were significantly reduced in YY PRKOX seeds (Supplemental Data Set 6A-C), and this could limit lipid accumulation despite the accumulation of precursors for FA biosynthesis. Recent reports further indicate that enhanced FA trafficking from the plastids into the ER promotes seed lipid accumulation in Arabidopsis (Kim et al., 2013; Tian et al., 2018; Li et al., 2020).

Several observations suggest that more integrated modifications to seed carbon metabolism can have large influences on seed FA metabolism. Studies of the transcription factor WRI1 are illustrative of this phenomenon. Seeds of *wri1* show a drastic reduction in seed oil content alongside accumulation of soluble sugars, likely as a consequence of a largely affected transcriptional program that results in altered activities of the enzymes involved in glycolysis and FA biosynthesis (Focks and Benning, 1998; Ruuska et al., 2002; Baud and Graham, 2006; Baud et al., 2007). Constitutive and ectopic overexpression of WRI1 in Arabidopsis increased seed oil content, but also caused the accumulation of TAG in seedlings grown in the presence of

17

exogenous sugar sources (Cernac and Benning, 2004). Interestingly, the broad effects of WRI1 overexpression appear to be even more exploitable by simultaneous upregulation of TAG assembly (via DGAT expression) and disruption of TAG turnover (via lipase suppression), with the combined effect being stronger than either approach alone (Van Erp et al., 2014). Together, this indicates that the coordinated modulation of several factors and steps of lipid biosynthesis may be the most promising approach to increase seed oil content, which is consistent with our observations regarding the PRKOX line.

In conclusion, our observations provide genetic confirmation for the operation of the PRK/Rubisco shunt, and suggest that this pathway is tightly integrated with light harvesting and starch biosynthesis in the Arabidopsis embryo. We also show a potential for increasing the flux through the PRK/Rubisco shunt to provide more FA precursors, which, combined with other targeted interventions, could help increase lipid production in commercially important green oilseed species.

Materials and Methods

Plant material and growth conditions

Two independent *PRK* (AT1G32060) insertional mutants of *Arabidopsis thaliana* (Arabidopsis) were obtained from the European Arabidopsis Stock Centre. The *prk-1* T-DNA insertion mutant is from the GABI-KAT collection (GK-117E07) and was generated in the Columbia (Col-0) ecotype background. The *prk-2* transposon tagged line is from the RIKEN collection (RIKEN_pst19435) and is in the Nossen (No-0) ecotype background. The T-DNA and transposon insertions in exons four and two, respectively, were confirmed by PCR-based genotyping followed by Sanger sequencing of the resulting DNA bands.

For the assessment of seedling development, seeds were surface sterilized by a series of washes with first 4% [v/v] bleach and 0.6% [v/v] Tween20, then 70% [v/v] ethanol, and last sterile water. Seeds were subsequently resuspended in 0.1% [w/v] agar before being plated on solidified half-strength Murashige and Skoog (MS) medium. Seeds were stratified for 2 days at 4°C and subsequently grown for 12 days in regular 12h light and 12h dark cycles before phenotypic scoring.

Plants were grown on standard soil (Substrate 2 from Klasmann-Deilmann GmbH, Geeste, Germany). No additional fertilizer was applied during growth. The plants were grown in

1   a Kälte 3000 chamber illuminated with fluorescent bulbs (Master TL5 HO 39W/865, Philips,

2   Amsterdam, Netherlands) as the light source, under long-day conditions (16 h light per day), 150

3   µmol m^{-2} s^{-1} of light intensity (normal light) unless otherwise specified, at 20°C and 60% relative

4   humidity. Seeds were collected using clear Aracon tubes unless otherwise specified (Arasystem,

5   Ghent, Belgium), thus avoiding silique shading throughout development.

6

7   *Construction of transgenic lines and screening*

8   For cloning of the *PRK$_{pro}$:PRK-YFP* complementation construct, the promoter of *PRK*

9   (comprising 1.9 kb sequence upstream of the translation start at the AT1G32060 locus) was

10 cloned into a Gateway® pDONRTM P4P1r entry vector. The *PRK* coding sequence (excluding

11 the stop codon) was cloned into a Gateway® pDONRTM 221 entry vector. The coding sequence

12 for eYFP, cloned into a Gateway® pDONRTM P2rP3 entry vector, was as in Beeler et al., 2014.

13 Entry vectors were then recombined into the Gateway® destination vector pB7m34GW,0, which

14 contains a glufosinate resistance gene as a selectable marker. The final *PRK$_{pro}$:PRK-YFP*

15 expression vector was transformed into the *Agrobacterium tumefaciens* strain GV3101.

16 Heterozygous *prk-1* plants were transformed using the floral dip method (Clough and Bent,

17 1998; Zhang et al., 2006), and transformants were selected using the glufosinate resistance

18 marker of *PRK$_{pro}$:PRK-YFP*. Transgenic lines were pre-selected for a glufosinate resistance

19 segregation pattern of 3:1 (resistant:susceptible), consistent with a single-locus T-DNA insertion

20 in the T2 generation. Genomic DNA was extracted from T1 plant material and used for Illumina

21 whole-genome sequencing. A genome coverage of over 97% for all analyzed lines was obtained,

22 and overlapping reads containing both T-DNA borders and sequences matching the Col-0

23 reference genome were used to identify the loci of insertion. This was successful for four lines—

24 three were found to have the T-DNA inserted in a single genetic locus, and one had T-DNA

25 inserted at two loci with a strong genetic linkage. Molecular markers for confirming the insertion

26 sites and allowing classification at greater detail were designed for the first three lines. This

27 analysis allowed us to exclude another line due to the presence of a tandem insertion. Finally, for

28 all further experiments, we selected the one of the remaining two lines whose insertion was at the

29 greater distance from neighboring genes. The transgene insertion in this line is localized in an

30 intergenic region 1,258 base pairs (bp) upstream of the translation start of *AT3G24800*, which

31 encodes pyruvate phosphate dikinase (PPDK).

19

1

Seed dissection and screening

To discriminate *prk* embryos from embryos complemented with *PRK_{pro}:PRK-YFP*, dry mature seeds were imbibed for 2-4 h at 4°C in water, allowing us to remove the seed coats using tweezers. The fluorescence status of each embryo was identified using a Leica zoom microscope equipped with a GFP-LP filter (Leica #10447407, Filter set ET GFP LP - M205FA/M165FC, excitation 460 to 500 nm, emission 510 nm long-pass). Dissected embryos were kept on filter paper placed on an agar plate containing half-strength MS medium until further processing.

Purification of recombinant PRK protein for antibody generation

The *PRK* coding sequence, excluding the first 162 bp predicted to encode a transit peptide (Emanuelsson et al., 1999) and the stop codon, was PCR-amplified using primers containing *Eco*RI and *Xho*I restriction sites. The resulting DNA fragment was then cloned into the pET-21a vector (Novagen) in frame with sequence encoding a C-terminal 6XHis-tag, using its flanking restriction sites. Because early reports have indicated difficulties when expressing wild-type PRK in *Escherichia coli* (Hudson et al., 1992), we performed site-directed mutagenesis using the QuikChangeTM Site-Directed Mutagenesis Kit (Agilent, Santa Clara, USA) to replace the two redox-sensitive Cys residues (Porter and Hartman, 1990; Milanez et al., 1991) with Ser residues, and then transformed *E. coli* BL21 cells for heterologous expression.

Transformed cells were grown at 37°C and 260 rpm (Infors HT Multitron incubator) in LB medium containing ampicillin (50 µg mL^{-1}) and chloramphenicol (12.5 µg mL^{-1}) to an optical density (OD_{600}) of 0.5-0.8. Protein expression was induced by adding isopropyl *β*-D-1-thiogalactopyranoside (IPTG) to a final concentration of 1 mM, after which cells were incubated at 20°C for another 16 h. Cells were then pelleted by centrifugation for 10 min at 4°C and 3,107 *g* and then resuspended in lysis buffer (50 mM Tris-HCl, pH 8, 300 mM NaCl, 40 mM imidazole, 2 mM dithiothreitol (DTT), 1 mg mL^{-1} lysozyme and 1X cOmpleteTM Protease Inhibitor Cocktail (Roche, Switzerland)). Cells were passed through a microfluidizer three times and the resulting lysate was cleared by centrifugation for 10 min at 4°C and 20,400 *g*. The supernatant was incubated for 1 h with Protino® Ni-NTA Agarose (Macherey-Nagel, Düren, Germany). After a 1-min centrifugation at 4°C and 200 *g*, the agarose resin was resuspended in lysis buffer and washed five times with 50 mM Tris-HCl, pH 8, 300 mM NaCl, 40 mM

20

1   imidazole, 2 mM DTT, 0.5% [w/v] Triton X-100 and then five times with 50 mM Tris-HCl, pH

2   8, 300 mM NaCl, 40 mM imidazole, 2 mM DTT. Bound protein was eluted with elution buffers

3   containing 50 mM Tris-HCl, pH 8, 50 mM NaCl and a step-wise increasing concentration of

4   imidazole (100 mM, 250 mM, and 500 mM). Fractions for which protein could be detected by

5   Coomassie Brilliant Blue polyacrylamide gel electrophoresis (PAGE) were pooled and

6   concentrated using Amicon® Ultra Cell® 3k centrifugal filter units. Proteins were exchanged into a

7   buffer containing 50 mM Tris-HCl, pH 8, 10% [v/v] glycerol and 2 mM DTT using NAPTM-5

8   (GE Healthcare Life Sciences, Pittsburgh, USA) columns and were then stored at -80°C.

9   Rabbits were immunized using the recombinant protein as antigen by Eurogentec

10   (Seraing, Belgium). Antibodies were purified from serum using a two-step procedure first

11   enriching total IgG using Protein A-Agarose (Roche, Switzerland) and then selecting anti-PRK

12   antibodies by affinity purification using recombinant PRK protein coupled to an NHS-activated

13   High Performance column (GE Healthcare Life Sciences, Pittsburgh, USA). Antibodies were

14   concentrated using Amicon® Ultra Cell® 3k spin-filter units (Merck, Germany) and subsequently

15   stored at -80°C in 2.7 mM potassium chloride, 10 mM sodium hydrogen phosphate, 1.8 mM

16   potassium dihydrogen phosphate, pH 7.4. Purified antibodies were used at a dilution of 1:600 for

17   immunoblots (see below).

18

19   *Protein extraction and immunoblotting*

20   Plant material was homogenized in 500 mM Tris-HCl, pH 6.8, 30% [v/v] glycerol, 20% [w/v]

21   SDS, 1 M DTT, 0.05% [w/v] bromophenol blue in a buffer-to-tissue ratio of 10 μL per mg fresh

22   weight. After centrifugation (10,000 *g*, 5 min, 4°C), the supernatant was kept at -20°C. Proteins

23   were separated by SDS-PAGE and transferred to Immobilon-FL polyvinylidene fluoride (PVDF)

24   membranes (pore size 0.45 μm, Merck Millipore Ltd.). Membranes were dried briefly,

25   reactivated in methanol, and blocked in TBST (20 mM Tris-HCl, pH 7.4, 150 mM glycine, 0.1%

26   [v/v] TWEEN® 20) supplemented with 3% [w/v] skimmed milk powder for 1 h at 4°C.

27   Membranes were then incubated in TBST supplemented with 3% [w/v] skimmed milk powder

28   and appropriate primary antibodies (purified custom anti-PRK: 1:600; commercial GFP

29   antibody: Clontech JL-8: 1:5,000; commercial anti-plant-actin: Sigma-Aldrich, clone 10-B3:

30   1:10,000) for 16 h at 4°C, washed five times with TBST at room temperature, and incubated for

31   1 h at RT in TBST supplemented with 3% [w/v] skimmed milk powder, 0.1% [w/v] SDS, and

1 secondary antibodies (IRDye 680RD Donkey anti-Mouse IgG / IRDye 800CW Donkey anti-
2 Rabbit IgG at a dilution of 1:20,000). Membranes were then washed five times with TBST and
3 imaged with a Li-Cor Odyssey System, allowing the fluorochromes coupled to the secondary
4 antibodies to be detected simultaneously.

5

6 *Metabolite extraction and LC-MS measurements*
7 Green seeds from single siliques were screened, collected in Eppendorf tubes, and deep-frozen in
8 liquid N_2. Samples were homogenised in 250 μL chloroform:methanol 3:7 [v:v] mixture using a
9 plastic pestle and incubated for 2 h at -20°C, with brief vortexing every 30 min. Three
10 extractions with each 400 μL of H_2O, each followed by centrifugation (16,000 *g*, 5 min, 4°C),
11 were done on each sample, the aqueous supernatants collected and dried using an Eppendorf
12 Concentrator plus (30°C), and stored at -80°C until the measurements (Arrivault et al., 2009).
13 Samples were then dissolved in 100 μL H_2O, filtered through a 0.2-μm Minisart® RC4
14 Regenerated Cellulose Syringe Filter (Sartorius AG, Germany), and analysed using a UHPLC-
15 MS/MS configuration consisting of a 1290 Infinity UHPLC (Agilent, Santa Clara, USA)
16 equipped with an Acquity T3 end-capped reverse phase column (Waters, Milford, USA) that was
17 coupled to a QTRAP 5500 triple quadrupole MS (AB Sciex, Framingham, USA) (Buescher et
18 al., 2010).

19 Data were analysed using Multiquant 3.03, ABSciex and relevant metabolites selected for
20 further analysis. Among these, metabolite contents below the dynamic range of the calibration
21 curve were utilized as such, whereas those for which no peak could be integrated were set to the
22 minimum value of the entire dataset times 10^{-3} to allow $\log_{10}$-transformation (See Supplemental
23 Data Sets 1 and 6 for details; also note that the metabolite analyses for prkCOMP and PRKOX
24 originate from the same dataset and thus share the same minimum value). Log_{10}-transformed
25 data were used for PCA analysis using the R packages FactoMineR (Lê et al., 2008) and
26 factoextra (Kassambara and Mundt, 2017), and for statistical analyses using GraphPad Prism,
27 version 9.3.1, for macOS.

28

29 *Lipid quantification*
30 FAME were prepared to perform an absolute quantification of the lipid content according to
31 Miquel and Browse (1992). From mature dry seeds, dissected material was transferred into a

1 mixture of methanol:toluene 2:1 [v:v], 2.5% [v:v] H_2SO_4, 2% [v:v] dimethoxypropane

2 containing 20 µg of tripentadecanoate (Merck KGaA, Darmstadt, Germany) as internal standard

3 for later quantification. After creating an argon atmosphere, tubes were heated to 80°C for 60

4 min. Cooled samples were neutralized with 100 mM Tris-HCl, pH 8, 0.9% [w/v] NaCl. After

5 two extractions with hexane, the pooled supernatants were dried under a nitrogen flow and

6 dissolved in 100 µL acetonitrile. FAME extracts were subsequently separated by gas

7 chromatography (GC) on a DB-23 column (30 m x 0.25 mm; 0.25 µm coating thickness; J&W

8 Scientific, Agilent, Waldbronn, Germany) followed by detection using a flame ionization

9 detector (FID) according to Lang et al. (2011). The GC program was as follows: 1 min at 150°C,

10 increase to 200°C at a rate of 8°C min^{-1}, increase to 250°C at a rate of 25°C min^{-1}. Total FA

11 content is defined as the sum of 17 FAME species: 16:0, 16:1 (9*Z*), 18:0, 18:1 (9*Z*), 18:1 (11*Z*),

12 18:2 (9*Z*, 12*Z*), 18:3 (9*Z*, 12*Z*, 15*Z*), 20:0, 20:1 (11*Z*), 20:1 (13*Z*), 20:2 (11*Z*, 14*Z*), 20:3 (11*Z*,

13 14*Z*, 17*Z*), 22:0, 22:1 (13*Z*), 22:2 (13*Z*, 15*Z*), 24:0 and 24:1 (15*Z*). Identification of individual

14 FAME species was done using a custom standard FAME mixture (FAME Mix, C4-C24, Merck

15 KGaA, Darmstadt, Germany). FAME quantifications were calculated from extrapolation based

16 on the internal standard.

17

18 *Chlorophyll measurements*

19 Chlorophylls from pooled seeds were extracted in 80% [v/v] acetone at 1 µL seed^{-1} for 24 h in

20 the dark at 4°C. Absorbances at 664 nm and 647 nm were then measured in the supernatant using

21 a nano-drop spectrophotometer (NanoDrop ND-1000) set to UV/Vis mode, using 80% [v/v]

22 acetone as a blank. Total chlorophyll was calculated from A_{664} and A_{647} as described previously

23 (Inskeep and Bloom, 1985). The remaining acetone was then removed and the seed samples were

24 used for starch measurements (see below; samples were stored at -20°C until further processing).

25

26 *Starch measurements*

27 Seeds were ground in 40 µL of H_2O, then two 10 µL aliquots per sample were separately

28 incubated at 100°C for 10 min. Samples were allowed to cool to room temperature (~22°C) for

29 10 min before addition of 10 µL of AA/AMG solution to one (digest) and 10 µL of control

30 solution to the other (control) aliquot of each original sample. AA/AMG solution consisted of 2.6

31 µL (~26 units) α-amylase (Roche) and 23.4 µL (~3.3 units) of amyloglucosidase (Roche) in a

23

1 final volume of 520 µL with 50 mM sodium acetate, pH 4.8, and the control solution contained

2 50 mM sodium acetate, pH 4.8 with water added at the same ratio as enzyme for AA/AMG.

3 Digested samples and undigested controls were then incubated for 4 h at 37°C before

4 quantification of free glucose (Glc) using glucose oxidase (GlcOx), horse radish peroxidase

5 (HRP), and Ampliflu-red (Amp-Red) as described previously (Solhaug et al., 2019). The Amp-

6 Red glucose assay solution was prepared by combining 1 µL of Amp-Red (Sigma; 10 mM

7 dissolved in DMSO), 1 µL GlcOx (Fluka; 0.1 units), 1 µL HRP (Fluka; 0.1 units), 5.6 µL sodium

8 phosphate buffer (150 mM, pH 7.4), and made up to 25 µL with DI H_2O. Samples were mixed

9 with 150 mM sodium phosphate pH 7.4, H_2O, and Amp-Red glucose assay solution at a 1:1:1:1

10 ratio. After combining all components, reactions were incubated at room temperature (~22°C) in

11 the dark for 25 min before measuring absorbances at 570 nm (A_{570}). Due to the segregation into

12 high- and low-starch content classes, absorbances had to be measured using different devices.

13 Samples with low glucose content were measured using the UV/Vis function of a nano-drop

14 spectrophotometer, whereas samples with high glucose content were measured using a

15 microplate reader (Tecan infinite M1000). The quantity of Glc produced from starch was

16 determined from the ΔA_{570} of the respective measurements of digested and undigested control

17 samples, using a standard curve of D-glucose ($0 - 500$ µM) as a reference.

18

19 *Sample preparation for TEM and imaging*

20 Green embryos were sorted, chemically fixed in 100 mM Na-cacodylate, pH 7.4, 2.5% [v/v]

21 glutaraldehyde, and 2% [w/v] formaldehyde. Samples were washed three times with 100 mM

22 Na-cacodylate, pH 7.4, and then stained with 1% [w/v] osmium (VIII) tetroxide in 100 mM Na-

23 cacodylate, pH 7.4. Samples were washed with H_2O and dehydrated in an aqueous dilution series

24 of ethanol (50%, 60%, 70%, 80%, 98%, 3 x 100%). Samples were then infiltrated with Spurr

25 (Polysciences) resin (2 x 25%, 2 x 50%, 2 x 75%, 3 x 100%; Spurr dilutions in dehydrated

26 ethanol). All steps were done using a Pelco Biowave® Pro+. Resin blocks were polymerized at

27 60°C for 2 days, and 70 nm thin sections cut using an ultramicrotome (Leica Ultracut E).

28 Sections were incubated with 2% [w/v] uranyl acetate and Reynold's solution (1.33 g $Pb(NO_3)_2$,

29 1.76 g Na_3 ($C_6H_5O_7$) $2H_2O$, 30 mL distilled water; Reynolds, 1963) for 10 min each, with 4

30 washes of water in between and afterwards. TEM micrographs were acquired using a JEOL

31 JEM-1400 Flash Electron Microscope.

1

Accession Numbers

Arabidopsis *PRK,* AT1G32060. Germplasm used: *prk-1* T-DNA insertion mutant, GK-117E07,

Columbia (Col-0) background; *prk-2* transposon mutant, RIKEN_pst19435, Nossen (No-0)

background.

6

Table 1: Segregation analysis of green versus pale seedlings germinating from seeds of a
heterozygous *prk-1* mother plant. Seeds were germinated on half-strength MS plates and grown
under regular 12h light / 12 h dark cycles for 12 days before classifying them as either green or
pale.

Mother plant	Green seedlings	Pale seedlings	Non-germinating	Total
Col-0	164 (100%)	0	0	164
Heterozygous *prk-1*	484 (74.6%)	163 (25.1%)	2 (0.3%)	649

11

Supplemental Data

Supplemental Figure 1. Near-endogenous expression levels of PRK-YFP in one-month old

prkCOMP rosette leaves, and prkCOMP/PRKOX growth (Supports Figures 2A and C).

Supplemental Figure 2. The PRK/Rubisco shunt and changes in the involved metabolites upon

overexpression of PRK in green embryos (Supports Figures 4 and 5A).

Supplemental Table 1. Analysis of individual FA species in sorted prkCOMP embryos.

Supplemental Table 2. Oligonucleotide primers used in this study.

Supplemental Data Set 1. LC-MS based quantification of selected metabolites in green

prkCOMP seeds.

Supplemental Data Set 2. FA quantification in sorted, mature WT, prkCOMP, and PRKOX

embryos.

Supplemental Data Set 3. FA quantification in sorted, mature prkCOMP embryos grown under

different light conditions.

Supplemental Data Set 4. Chlorophyll measurements of sorted, green prkCOMP seeds.

Supplemental Data Set 5. Starch content measurements of sorted, green prkCOMP seeds.

Supplemental Data Set 6. LC-MS based quantification of selected metabolites in green PRKOX

seeds.

25

1

16

17   **Figure Legends**

18   **Figure 1.** Mutations disrupting PRK are seedling-lethal.

19   **A** Structure of the *PRK* locus (AT1G32060.1) depicting untranslated regions (magenta), introns

20   (black), and exons (cyan). The region encoding the transit peptide of 54 amino acid residues, as

21   predicted by ChloroP (Emanuelsson et al. 1999), is marked with a grey dashed box. The

22   locations of the T-DNA (*prk-1*) and transposon (*prk-2*) insertions are indicated by triangles. **B**

23   Seeds and 12-d-old seedlings derived from selfed heterozygous *prk-1* and *prk-2* mother plants in

24   comparison to the respective wild-type accessions (Col-0 for *prk-1*, No-0 for *prk-2*). The

25   homozygous *prk* seedlings are pale and do not develop beyond the cotyledon stage. Bars = 1

26   mm.

27

28   **Figure 2.** Hemizygous PRK-YFP expression rescues the *prk* growth phenotype and allows

29   selection of homozygous *prk* seeds.

30   **A** Immunoblot using extracts of 10-d old Col-0 WT and prkCOMP seedlings, showing

31   expression of PRK-YFP and lack of endogenous PRK in the segregating population. Seedlings

were sorted according to their growth phenotype (Green versus Pale; compare Figure 1B). Protein was loaded on an equal fresh weight basis (500 ng per lane). The upper blot displays the cumulative signal of two color channels from anti-PRK and anti-YFP antibodies, whereas actin was used as a loading control in the lower blot and is shown in red. **B** Segregating populations of green seeds harvested at different stages (DAF: days after flowering) from individual prkCOMP siliques. Seeds classified as "R" according to the fluorescence sorting are marked with magenta arrowheads. Bars = 1 mm. **C** Immunoblot of Col-0 WT and sorted green prkCOMP seeds harvested 10 DAF, showing absence of endogenous PRK and presence of PRK-YFP at levels positively correlated with YFP fluorescence in complemented seeds. Protein equivalents to 0.83 seed are loaded per lane; actin was used as a loading control and is shown in red.

Figure 3. PCA analysis of primary metabolites measured in sorted green prkCOMP seeds.

Biplot for principal components 1 and 2. Siliques ($n = 19$) were opened, the seeds therein sorted and pooled according to fluorescence (6-38 seeds per pool sample in the displayed dataset), and metabolites quantified. Small circles represent individual samples and are colored according to their assigned fluorescence class. Large circles represent group mean points and lightly shaded ellipses are concentration ellipses assuming a multivariate normal distribution, drawn to a normal probability of 68%. Metabolite variables are colored and faded according to their contribution. See Supplemental Data Set 1A for raw metabolite data.

Figure 4. The PRK/Rubisco shunt and changes in the involved metabolites upon loss of *prk* in green seeds.

The upper part of the scheme shows the canonical glycolysis pathway. The lower part shows how enzymes of the nonoxidative steps of the pentose phosphate pathway (PPP), together with PRK and Rubisco acting outside the CBBC, bypass parts of glycolysis (indicated in orange) and recycle CO_2 released by PDH in green Brassicaceae seeds (scheme adapted from Schwender et al., 2004). The relative changes in the mean metabolite levels in R seeds with respect to complemented YY seeds (R/YY; same underlying data as shown in Figure 3) originating from hemizygous prkCOMP mother plants are highlighted with colored boxes ($\log_{10}$ scale; see color legend). The value for RuBP was outside the displayed range, with a roughly 19-fold reduction. Statistically significant increases or decreases are indicated by asterisks; **, $p < 0.01$; ***, $p <$

27

1 0.001 represent p values from 2-way ANOVA adjusted for multiple comparisons according to

2 the Šidák method. Metabolites that were not analyzed are displayed in grey. See Supplemental

3 Data Set 1B and C for statistical analyses and relative metabolite changes, respectively.

4 Metabolites: ADPGlc, ADP-glucose; DHAP, dihydroxyacetone phosphate; Ery4P, erythrose-4-

5 phosphate; FruBP, fructose-1,6-bisphosphate; Fru6P, fructose-6-phosphate; GAP,

6 glyceraldehyde-3-phosphate; Glc1P, glucose-1-phosphate; Glc6P, glucose-6-phosphate; PEP,

7 phosphoenolpyruvate; Pyr, pyruvate; Rib5P, ribose-5-phosphate; RuBP, ribulose bisphosphate;

8 Sed7P, sedoheptulose-7-phosphate; Xyl5P, xylulose-5-phosphate; 1,3BPG, 1,3-

9 bisphosphoglycerate; 2PGA, 2-phosphoglycerate; 3PGA, 3-phosphoglycerate. Enzymes: Aldo,

10 FruBP aldolase; Eno, 2PGA enolase; GAPDH, GAP dehydrogenase; PFK, phosphofructokinase;

11 PGI, phosphoglucose isomerase; PGK, phosphoglycerate kinase; PGM, phosphoglyceromutase;

12 PK, Pyr kinase; Riso, Rib5P isomerase; TK, transketolase; TPI, triose phosphate isomerase;

13 Xepi; Xyl5P epimerase.

14

15 **Figure 5.** FA quantification in embryos dissected from mature seeds.

16 **A** FA contents of sorted embryos excised from prkCOMP, PRKOX, and Col-0 WT seeds.

17 Mature, imbibed seeds were dissected and embryos were sorted according to their fluorescence

18 (no distinction was made between Y and YY samples). FAs were extracted and measured using

19 GC-FID. Values displayed are mean total FA contents on a per-embryo basis (black bar outline)

20 and mean contribution of different FA species to the total content in color. Individual biological

21 replicates (*n*) consisted of pools of several (5-10) embryos. *N* = number of mother plants whose

22 seeds were sampled. Error bars represent the standard error of the mean (SEM). ns, not

23 significant ($p > 0.05$); ***, $p < 0.001$ based on two-tailed t-tests for homoscedastic groups. See

24 Supplemental Data Set 2 for FA quantifications and a statistical analysis of total FA contents. **B**

25 FA content of sorted prkCOMP and Col-0 WT embryos in relation to light intensity perceived

26 during development. Mother plants were grown at high light intensity (HL: 300 µmol m^{-2} s^{-1}).

27 Grey filters reducing light intensity by 50% to normal light (150 µmol m^{-2} s^{-1}) either on only the

28 mother plant's rosettes (NLr samples) or the entire mother plant (including developing siliques;

29 NL samples) were installed near the time of bolting. Mature seeds were dissected, sorted, and

30 extracted as in A; data display is as in A. *, $p < 0.05$; **, $p < 0.01$; *** $p < 0.001$ based on Welch

31 ANOVA with Dunnett's T3 correction for multiple comparisons. See Supplemental Data Set 3A

28

and 3B for FA quantifications and a statistical analysis of total FA contents, respectively. In both A and B, individual data points are scattered over the bars, with matching colors representing the same mother plant.

Figure 6. Chlorophyll content of sorted green prkCOMP seeds.

Values displayed are the total chlorophyll contents of R and YY seeds. Samples ($n = 11$) consisted of pooled seeds (11-22) from the same silique. The asterisk represents a statistically significant difference (*, $p < 0.05$) between the two groups based on a two-tailed paired t-test. See Supplemental Data Set 4 for chlorophyll quantifications and a statistical analysis thereof.

Figure 7. Visualization of lipid bodies and starch in green *prk* and complemented embryos.

A TEMs of thin sections of resin-embedded prkCOMP embryos harvested and dissected 4 h into the day. At 13 DAF, starch granules (S) were present in plastids of both *prk* (R) and the complemented (YY) siblings (upper micrographs; similar observations were made at 7 DAF in another experimental batch). At 16 DAF, starch granules were still present in *prk* embryos, but largely absent in YY embryos (lower micrographs). Bar = 2 μm. **B** Enlarged regions of 16 DAF micrographs (from the dotted rectangles in A). Green dashed outlines indicate plastids; S, starch granules; O, oil bodies. Bar = 1 μm. Parts A and B show representative images of more than ten images taken for each section. **C** Starch measurements of sorted green prkCOMP seeds harvested at 11 DAF. Values displayed are the starch contents of R seeds normalized to the respective YY sample from the same silique. Siliques segregated into two classes with either high (> 15 nmols seed^{-1}) or low starch content, possibly due to small differences in their developmental stages. This classification of samples is indicated by the color of individual data points. Samples (n) consisted of pools of seeds (11-22) from the same silique. All siliques originated from the same mother plant. The asterisk represents a statistically significant difference (*, $p < 0.05$) against the null hypothesis $\mu_0 = 1$ (indicated as yellow dashed line), based on a two-tailed t-test. See Supplemental Data Set 5 for starch quantifications and the statistical analysis thereof.

29

1

2   **References**

3   **Andersson, I., and Backlund, A.** (2008). Structure and function of Rubisco. Plant Physiology
4   and Biochemistry **46,** 275-291.

5   **Andriotis, V.M., Pike, M.J., Kular, B., Rawsthorne, S., and Smith, A.M.** (2010). Starch
6   turnover in developing oilseed embryos. New Phytologist **187,** 791-804.

7   **Andriotis, V.M., Pike, M.J., Schwarz, S.L., Rawsthorne, S., Wang, T.L., and Smith, A.M.**
8   (2012). Altered starch turnover in the maternal plant has major effects on Arabidopsis
9   fruit growth and seed composition. Plant Physiology **160,** 1175-1186.

10 **Arrivault, S., Guenther, M., Ivakov, A., Feil, R., Vosloh, D., Van Dongen, J.T., Sulpice, R.,**
11   **and Stitt, M.** (2009). Use of reverse‑phase liquid chromatography, linked to tandem
12   mass spectrometry, to profile the Calvin cycle and other metabolic intermediates in
13   Arabidopsis rosettes at different carbon dioxide concentrations. The Plant Journal **59,**
14   826-839.

15 **Asokanthan, P.S., Johnson, R.W., Griffith, M., and Krol, M.** (1997). The photosynthetic
16   potential of canola embryos. Physiologia Plantarum **101,** 353-360.

17 **Banks, F.M., Driscoll, S.P., Parry, M.A., Lawlor, D.W., Knight, J.S., Gray, J.C., and Paul,**
18   **M.J.** (1999). Decrease in phosphoribulokinase activity by antisense RNA in transgenic
19   tobacco. Relationship between photosynthesis, growth, and allocation at different
20   nitrogen levels. Plant Physiology **119,** 1125-1136.

21 **Bates, P.D., Stymne, S., and Ohlrogge, J.** (2013). Biochemical pathways in seed oil synthesis.
22   Current opinion in plant biology **16,** 358-364.

23 **Baud, S., and Graham, I.A.** (2006). A spatiotemporal analysis of enzymatic activities
24   associated with carbon metabolism in wild‑type and mutant embryos of Arabidopsis
25   using in situ histochemistry. The Plant Journal **46,** 155-169.

26 **Baud, S., and Lepiniec, L.** (2010). Physiological and developmental regulation of seed oil
27   production. Progress in lipid research **49,** 235-249.

28 **Baud, S., Boutin, J.-P., Miquel, M., Lepiniec, L., and Rochat, C.** (2002). An integrated
29   overview of seed development in Arabidopsis thaliana ecotype WS. Plant Physiology and
30   Biochemistry **40,** 151-160.

30

Baud, S., Dubreucq, B., Miquel, M., Rochat, C., and Lepiniec, L. (2008). Storage reserve accumulation in Arabidopsis: metabolic and developmental control of seed filling. The Arabidopsis book/American Society of Plant Biologists **6**.

Baud, S., Mendoza, M.S., To, A., Harscoët, E., Lepiniec, L., and Dubreucq, B. (2007). WRINKLED1 specifies the regulatory action of LEAFY COTYLEDON2 towards fatty acid metabolism during seed maturation in Arabidopsis. The Plant Journal **50,** 825-838.

Beeler, S., Liu, H.-C., Stadler, M., Schreier, T., Eicke, S., Lue, W.-L., Truernit, E., Zeeman, S.C., Chen, J., and Kötting, O. (2014). Plastidial NAD-dependent malate dehydrogenase is critical for embryo development and heterotrophic metabolism in Arabidopsis. Plant physiology **164,** 1175-1190.

Buescher, J.M., Moco, S., Sauer, U., and Zamboni, N. (2010). Ultrahigh performance liquid chromatography− tandem mass spectrometry method for fast and robust quantification of anionic and aromatic metabolites. Analytical chemistry **82,** 4403-4412.

Carrera, D.Á., George, G.M., Fischer-Stettler, M., Galbier, F., Eicke, S., Truernit, E., Streb, S., and Zeeman, S.C. (2021). Distinct plastid fructose bisphosphate aldolases function in photosynthetic and non-photosynthetic metabolism in Arabidopsis. Journal of experimental botany **72,** 3739-3755.

Cernac, A., and Benning, C. (2004). WRINKLED1 encodes an AP2/EREB domain protein involved in the control of storage compound biosynthesis in Arabidopsis. The Plant Journal **40,** 575-585.

Clough, S.J., and Bent, A.F. (1998). Floral dip: a simplified method for Agrobacterium‑mediated transformation of Arabidopsis thaliana. The plant journal **16,** 735-743.

da Silva, P.M., Eastmond, P.J., Hill, L.M., Smith, A.M., and Rawsthorne, S. (1997). Starch metabolism in developing embryos of oilseed rape. Planta **203,** 480-487.

Dehesh, K., Tai, H., Edwards, P., Byrne, J., and Jaworski, J.G. (2001). Overexpression of 3-ketoacyl-acyl-carrier protein synthase IIIs in plants reduces the rate of lipid synthesis. Plant physiology **125,** 1103-1114.

Eastmond, P., Koláčá, L., and Rawsthorne, S. (1996). Photosynthesis by developing embryos of oilseed rape (Brassica napus L.). Journal of Experimental Botany **47,** 1763-1769.

Eastmond, P.J., and Rawsthorne, S. (2000). Coordinate changes in carbon partitioning and plastidial metabolism during the development of oilseed rape embryos. Plant Physiology **122,** 767-774.

Emanuelsson, O., Nielsen, H., and Von Heijne, G. (1999). ChloroP, a neural network-based method for predicting chloroplast transit peptides and their cleavage sites. Protein Science **8,** 978-984.

Focks, N., and Benning, C. (1998). wrinkled1: a novel, low-seed-oil mutant of Arabidopsis with a deficiency in the seed-specific regulation of carbohydrate metabolism. Plant physiology **118,** 91-101.

Gardemann, A., Stitt, M., and Heldt, H. (1983). Control of CO2 fixation. Regulation of spinach ribulose-5-phosphate kinase by stromal metabolite levels. Biochimica et Biophysica Acta (BBA)-Bioenergetics **722,** 51-60.

Goffman, F.D., Alonso, A.P., Schwender, J., Shachar-Hill, Y., and Ohlrogge, J.B. (2005). Light enables a very high efficiency of carbon storage in developing embryos of rapeseed. Plant Physiology **138,** 2269-2279.

Hajduch, M., Casteel, J.E., Hurrelmeyer, K.E., Song, Z., Agrawal, G.K., and Thelen, J.J. (2006). Proteomic analysis of seed filling in Brassica napus. Developmental characterization of metabolic isozymes using high-resolution two-dimensional gel electrophoresis. Plant Physiology **141,** 32-46.

Hudson, G., Morell, M., Arvidsson, Y., and Andrews, T. (1992). Synthesis of spinach phosphoribulokinase and ribulose 1, 5-bisphosphate in Escherichia coli. Functional Plant Biology **19,** 213-221.

Iglesias, A., Barry, G., Meyer, C., Bloksberg, L., Nakata, P., Greene, T., Laughlin, M., Okita, T., Kishore, G., and Preiss, J. (1993). Expression of the potato tuber ADP-glucose pyrophosphorylase in Escherichia coli. Journal of Biological Chemistry **268,** 1081-1086.

Inskeep, W.P., and Bloom, P.R. (1985). Extinction coefficients of chlorophyll a and b in N, N-dimethylformamide and 80% acetone. Plant physiology **77,** 483-485.

Jako, C., Kumar, A., Wei, Y., Zou, J., Barton, D.L., Giblin, E.M., Covello, P.S., and Taylor, D.C. (2001). Seed-specific over-expression of an Arabidopsis cDNA encoding a

diacylglycerol acyltransferase enhances seed oil content and seed weight. Plant physiology **126,** 861-874.

Kang, F., and Rawsthorne, S. (1994). Starch and fatty acid synthesis in plastids from developing embryos of oilseed rape (Brassica napus L.). The Plant Journal **6,** 795-805.

Kassambara, A., and Mundt, F. (2017). Package factoextra: Extract and visualize the Results of Multivariate Data Analyses. R Package Version 1.0. 7.

Kim, S., Yamaoka, Y., Ono, H., Kim, H., Shim, D., Maeshima, M., Martinoia, E., Cahoon, E.B., Nishida, I., and Lee, Y. (2013). AtABCA9 transporter supplies fatty acids for lipid synthesis to the endoplasmic reticulum. Proceedings of the national academy of sciences **110,** 773-778.

King, S.P., Badger, M.R., and Furbank, R.T. (1998). CO2 refixation characteristics of developing canola seeds and silique wall. Functional Plant Biology **25,** 377-386.

Konishi, T., Shinohara, K., Yamada, K., and Sasaki, Y. (1996). Acetyl-CoA carboxylase in higher plants: most plants other than gramineae have both the prokaryotic and the eukaryotic forms of this enzyme. Plant and Cell Physiology **37,** 117-122.

Lang, I., Hodac, L., Friedl, T., and Feussner, I. (2011). Fatty acid profiles and their distribution patterns in microalgae: a comprehensive analysis of more than 2000 strains from the SAG culture collection. BMC plant biology **11,** 1-16.

Lê, S., Josse, J., and Husson, F. (2008). FactoMineR: an R package for multivariate analysis. Journal of statistical software **25,** 1-18.

Lemieux, B., Miquel, M., and Somerville, C. (1990). Mutants of Arabidopsis with alterations in seed lipid fatty acid composition. Theoretical and applied genetics **80,** 234-240.

Li, N., Meng, H., Li, S., Zhang, Z., Zhao, X., Wang, S., Liu, A., Li, Q., Song, Q., and Li, X. (2020). Two plastid fatty acid exporters contribute to seed oil accumulation in Arabidopsis. Plant Physiology **182,** 1910-1919.

Li, Y., Beisson, F., Pollard, M., and Ohlrogge, J. (2006). Oil content of Arabidopsis seeds: the influence of seed anatomy, light and plant-to-plant variation. Phytochemistry **67,** 904-915.

Lonien, J., and Schwender, J. (2009). Analysis of metabolic flux phenotypes for two Arabidopsis mutants with severe impairment in seed storage lipid synthesis. Plant Physiology **151,** 1617-1634.

33

Milanez, S., Mural, R.J., and Hartman, F.C. (1991). Roles of cysteinyl residues of phosphoribulokinase as examined by site-directed mutagenesis. Journal of Biological Chemistry **266,** 10694-10699.

Miquel, M., and Browse, J. (1992). Arabidopsis mutants deficient in polyunsaturated fatty acid synthesis. Biochemical and genetic characterization of a plant oleoyl-phosphatidylcholine desaturase. Journal of Biological Chemistry **267,** 1502-1509.

Niyogi, K.K. (1999). Photoprotection revisited: genetic and molecular approaches. Annual review of plant physiology and plant molecular biology **50,** 333-359.

Paul, M.J., Knight, J.S., Habash, D., Parry, M.A., Lawlor, D.W., Barnes, S.A., Loynes, A., and Gray, J.C. (1995). Reduction in phosphoribulokinase activity by antisense RNA in transgenic tobacco: effect on CO2 assimilation and growth in low irradiance. The Plant Journal **7,** 535-542.

Periappuram, C., Steinhauer, L., Barton, D.L., Taylor, D.C., Chatson, B., and Zou, J. (2000). The plastidic phosphoglucomutase from Arabidopsis. A reversible enzyme reaction with an important role in metabolic control. Plant Physiology **122,** 1193-1200.

Pfister, B., and Zeeman, S.C. (2016). Formation of starch in plant cells. Cellular and Molecular Life Sciences **73,** 2781-2807.

Porter, M.A., and Hartman, F.C. (1990). Exploration of the function of a regulatory sulfhydryl of phosphoribulokinase from spinach. Archives of biochemistry and biophysics **281,** 330-334.

Ramli, U.S., Baker, D.S., Quant, P.A., and Harwood, J.L. (2002). Control analysis of lipid biosynthesis in tissue cultures from oil crops shows that flux control is shared between fatty acid synthesis and lipid assembly. Biochemical Journal **364,** 393-401.

Roesler, K., Shintani, D., Savage, L., Boddupalli, S., and Ohlrogge, J. (1997). Targeting of the Arabidopsis homomeric acetyl-coenzyme A carboxylase to plastids of rapeseeds. Plant physiology **113,** 75-81.

Ruuska, S.A., Schwender, J., and Ohlrogge, J.B. (2004). The capacity of green oilseeds to utilize photosynthesis to drive biosynthetic processes. Plant physiology **136,** 2700-2709.

Ruuska, S.A., Girke, T., Benning, C., and Ohlrogge, J.B. (2002). Contrapuntal networks of gene expression during Arabidopsis seed filling. The Plant Cell **14,** 1191-1206.

Schwender, J., Goffman, F., Ohlrogge, J.B., and Shachar-Hill, Y. (2004). Rubisco without the Calvin cycle improves the carbon efficiency of developing green seeds. Nature **432,** 779-782.

Schwender, J., Hebbelmann, I., Heinzel, N., Hildebrandt, T., Rogers, A., Naik, D., Klapperstück, M., Braun, H.-P., Schreiber, F., and Denolf, P. (2015). Quantitative multilevel analysis of central metabolism in developing oilseeds of oilseed rape during in vitro culture. Plant Physiology **168,** 828-848.

Singer, S.D., Chen, G., Mietkiewska, E., Tomasi, P., Jayawardhane, K., Dyer, J.M., and Weselake, R.J. (2016). Arabidopsis GPAT9 contributes to synthesis of intracellular glycerolipids but not surface lipids. Journal of experimental botany **67,** 4627-4638.

Solhaug, E.M., Roy, R., Chatt, E.C., Klinkenberg, P.M., Mohd‑Fadzil, N.A., Hampton, M., Nikolau, B.J., and Carter, C.J. (2019). An integrated transcriptomics and metabolomics analysis of the Cucurbita pepo nectary implicates key modules of primary metabolism involved in nectar synthesis and secretion. Plant Direct **3,** e00120.

Taylor, D.C., Katavic, V., Zou, J., MacKenzie, S.L., Keller, W.A., An, J., Friesen, W., Barton, D.L., Pedersen, K.K., and Michael Giblin, E. (2002). Field testing of transgenic rapeseed cv. Hero transformed with a yeast sn-2 acyltransferase results in increased oil content, erucic acid content and seed yield. Molecular Breeding **8,** 317-322.

Thelen, J.J., and Ohlrogge, J.B. (2002). Both antisense and sense expression of biotin carboxyl carrier protein isoform 2 inactivates the plastid acetyl‑coenzyme A carboxylase in Arabidopsis thaliana. The Plant Journal **32,** 419-431.

Tian, Y., Lv, X., Xie, G., Zhang, J., Xu, Y., and Chen, F. (2018). Seed-specific overexpression of AtFAX1 increases seed oil content in Arabidopsis. Biochemical and biophysical research communications **500,** 370-375.

Tsogtbaatar, E., Cocuron, J.-C., and Alonso, A.P. (2020). Non-conventional pathways enable pennycress (Thlaspi arvense L.) embryos to achieve high efficiency of oil biosynthesis. Journal of experimental botany **71,** 3037-3051.

Van Erp, H., Kelly, A.A., Menard, G., and Eastmond, P.J. (2014). Multigene engineering of triacylglycerol metabolism boosts seed oil content in Arabidopsis. Plant Physiology **165,** 30-36.

1 **Verwoert, I.I., van der Linden, K.H., Walsh, M.C., Nijkamp, H.J.J., and Stuitje, A.R.**
2   (1995). Modification of Brassica napus seed oil by expression of the Escherichia coli
3   fabH gene, encoding 3-ketoacyl-acyl carrier protein synthase III. Plant molecular biology
4   **27,** 875-886.
5 **Vigeolas, H., Waldeck, P., Zank, T., and Geigenberger, P.** (2007). Increasing seed oil content
6   in oil‑seed rape (Brassica napus L.) by over‑expression of a yeast glycerol‑3‑phosphate
7   dehydrogenase under the control of a seed‑specific promoter. Plant Biotechnology
8   Journal **5,** 431-441.
9 **Wang, M., Garneau, M.G., Poudel, A.N., Lamm, D., Koo, A.J., Bates, P.D., and Thelen, J.J.**
10   (2022). Overexpression of pea α‑carboxyltransferase in Arabidopsis and camelina
11   increases fatty acid synthesis leading to improved seed oil content. The Plant Journal **110,**
12   1035-1046.
13 **White, J.A., Todd, J., Newman, T., Focks, N., Girke, T., de Ilárduya, O.M., Jaworski, J.G.,**
14   **Ohlrogge, J.B., and Benning, C.** (2000). A new set of Arabidopsis expressed sequence
15   tags from developing seeds. The metabolic pathway from carbohydrates to seed oil. Plant
16   physiology **124,** 1582-1594.
17 **Zhang, X., Henriques, R., Lin, S.-S., Niu, Q.-W., and Chua, N.-H.** (2006). Agrobacterium-
18   mediated transformation of Arabidopsis thaliana using the floral dip method. Nature
19   protocols **1,** 641-646.
20 **Zou, J., Katavic, V., Giblin, E.M., Barton, D.L., MacKenzie, S.L., Keller, W.A., Hu, X., and**
21   **Taylor, D.C.** (1997). Modification of seed oil content and acyl composition in the
22   brassicaceae by expression of a yeast sn-2 acyltransferase gene. The Plant Cell **9,** 909-
23   923.
24
25
26

A

PRK (*AT1G32060.1*)

B

1
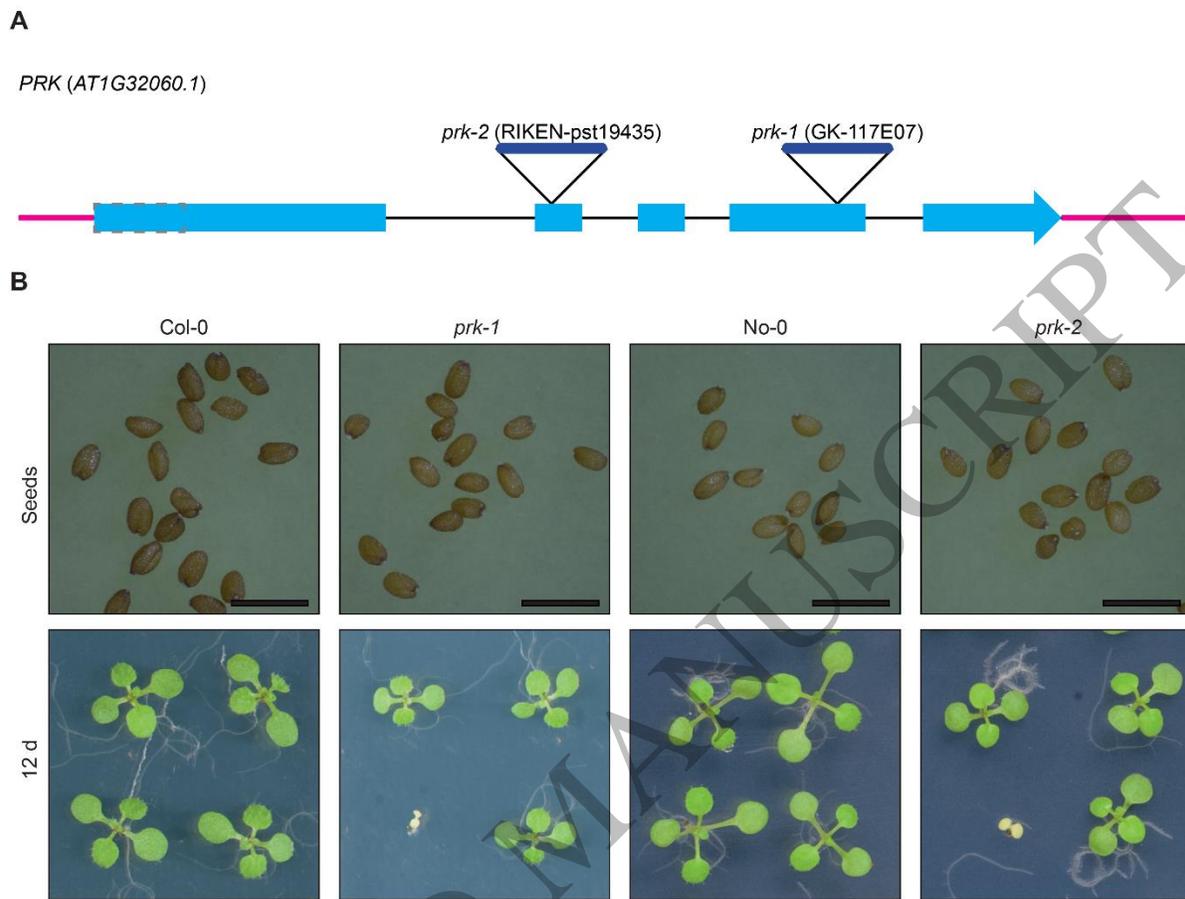
2   **Figure 1**

3   **159x121 mm (.38 x DPI)**

4
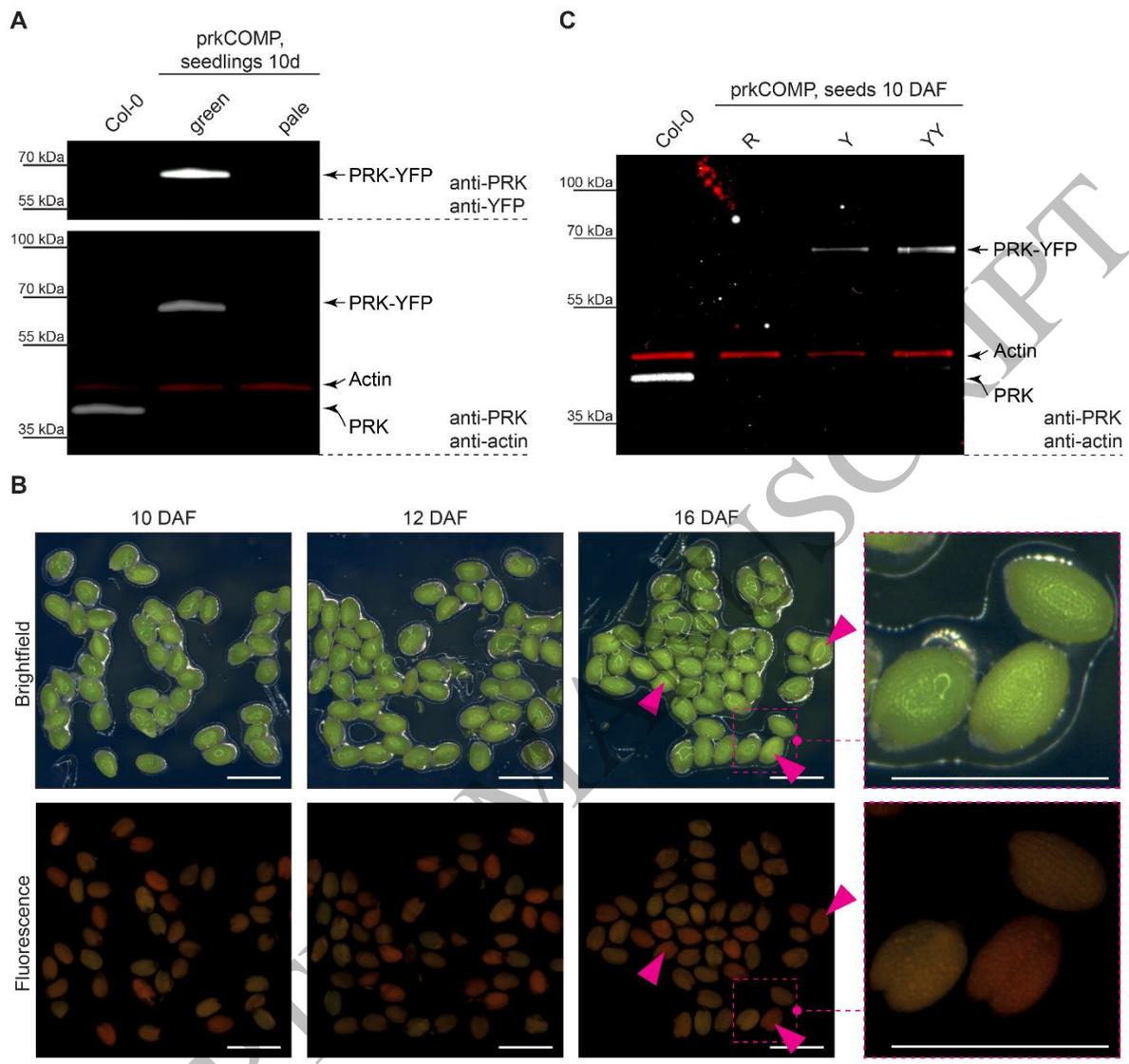
Figure 2
**159x150 mm (.38 x DPI)**
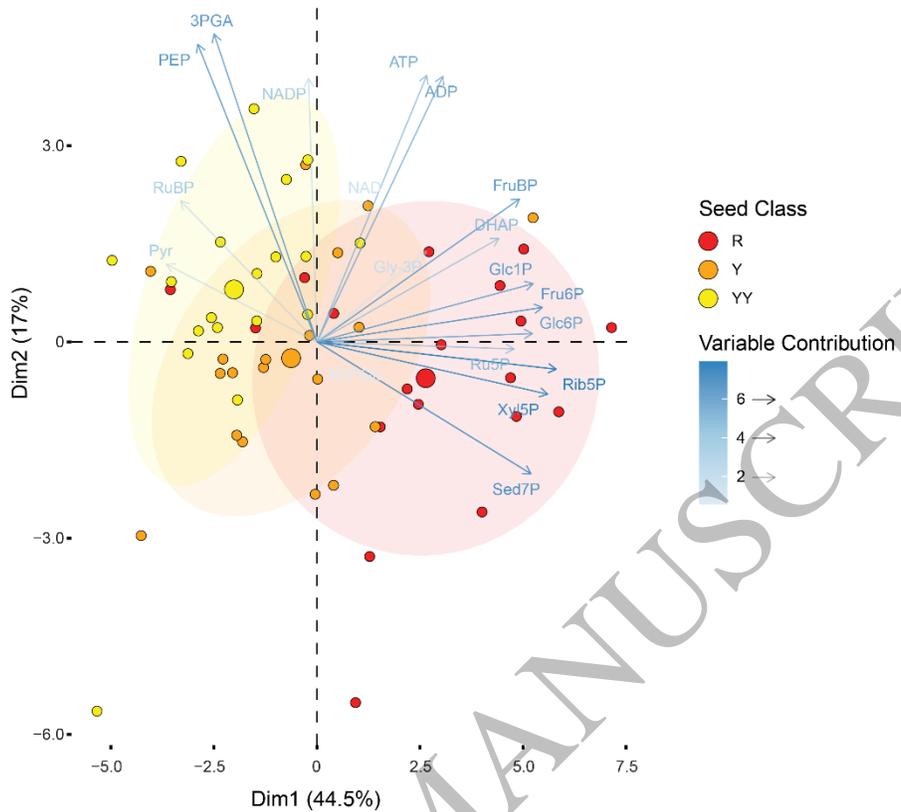
Figure 3
124x109 mm (.38 x DPI)
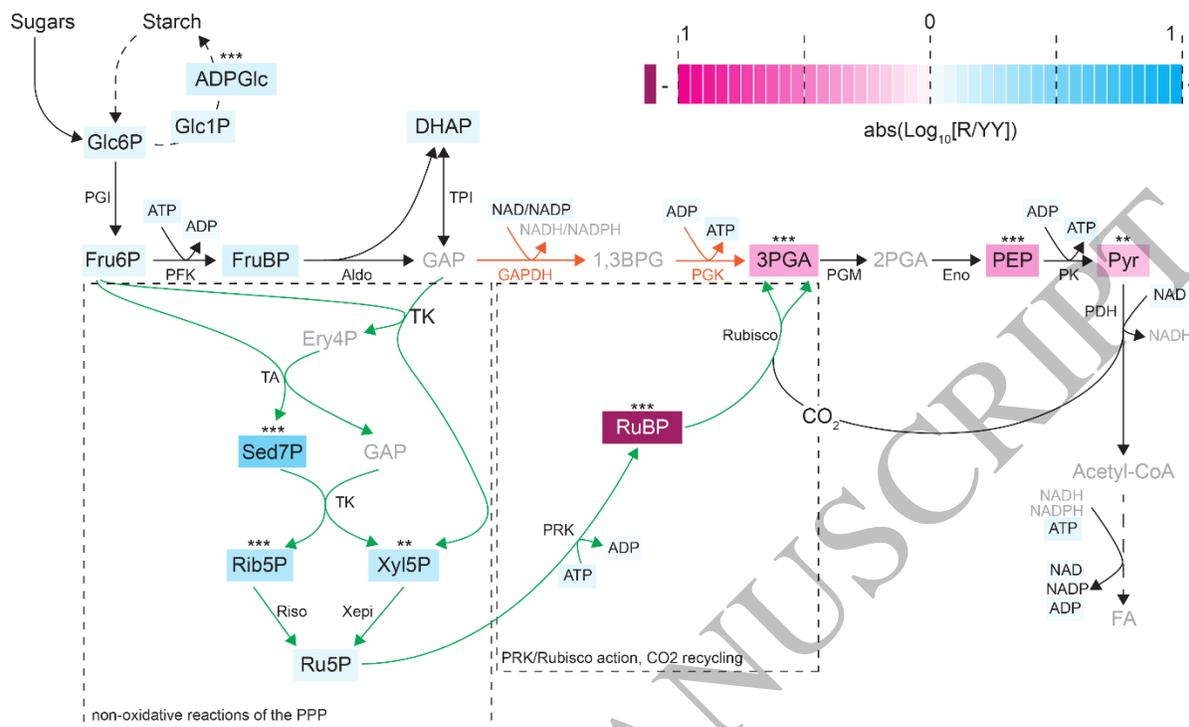
Figure 4
159x97 mm (.38 x DPI)
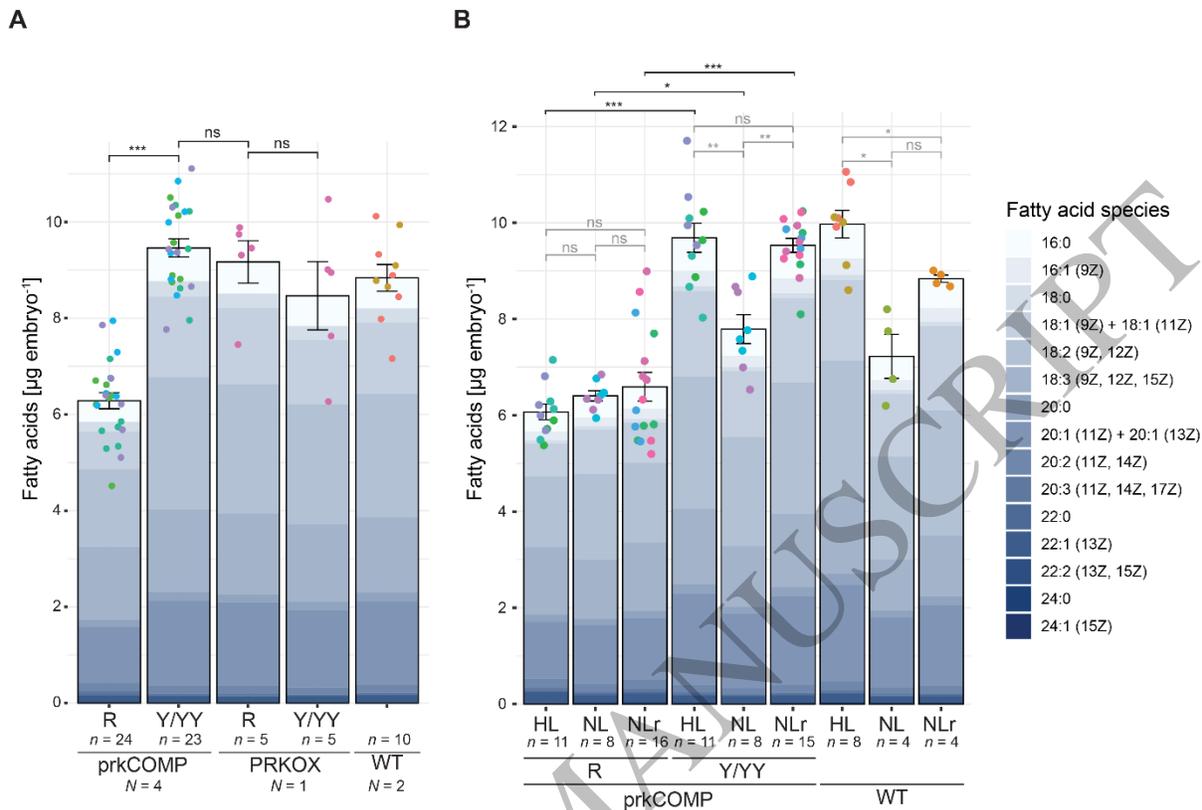
Figure 5
159x109 mm (.38 x DPI)
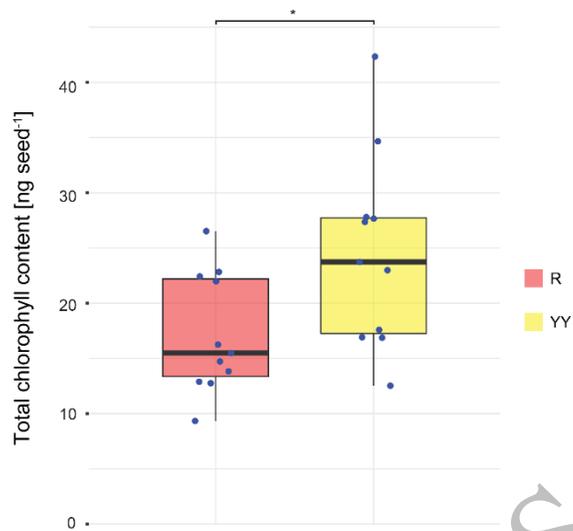
Figure 6
79x71 mm (.38 x DPI)

1

2
3

4

A prkCOMP

R YY

13 DAF

16 DAF

B

C

1

2
3
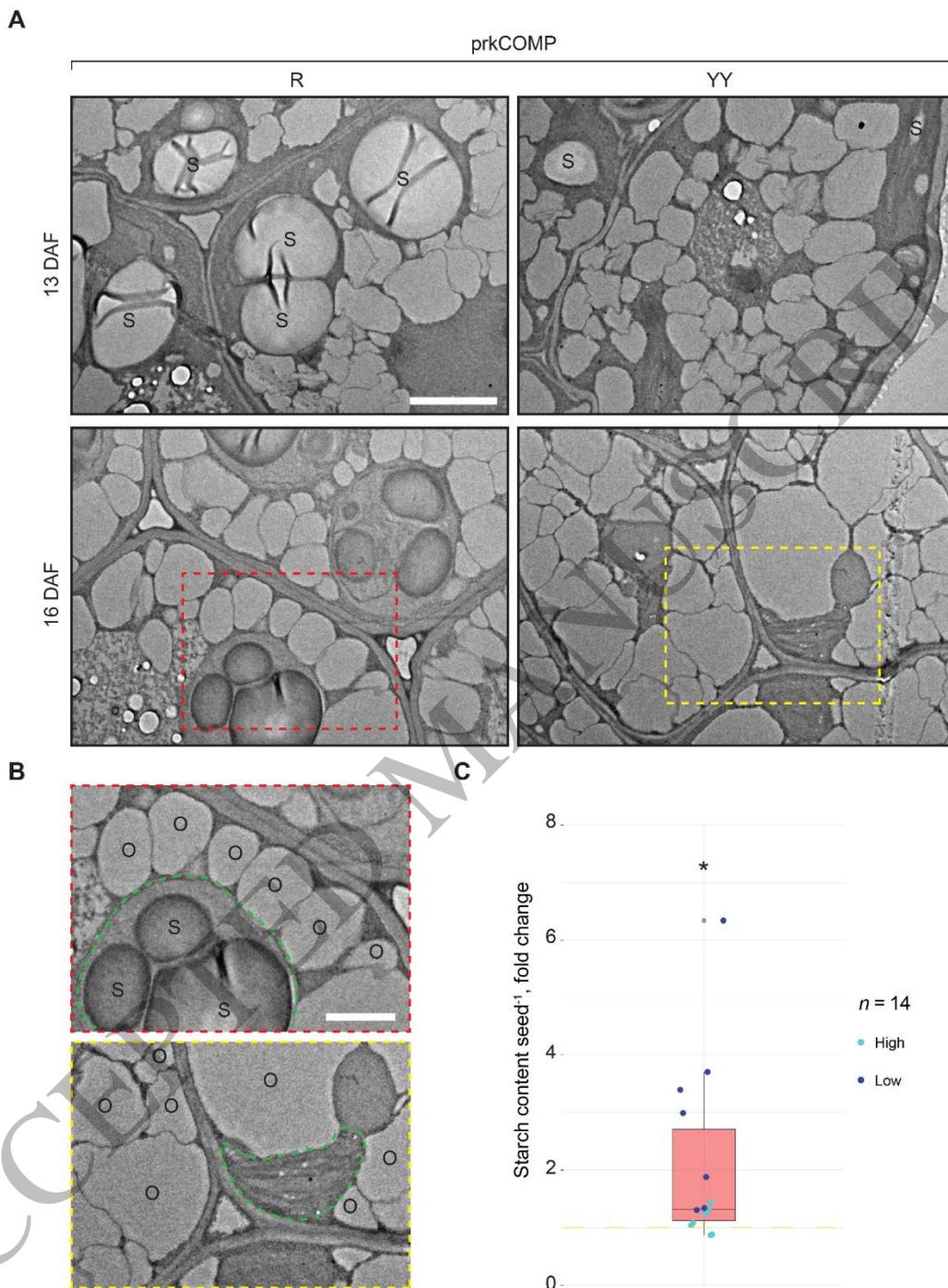
Figure 7
142x188 mm (.38 x DPI)